Nucleon Structure Study by Virtual Compton Scattering

N. D'Hose*, J.E. Ducret, Th. Gousset, P.A.M. Guichon, S. Kerhoas, D. Lhuillier, C. Marchand, D. Marchand, J. Martino, J. Mougey, J. Roche, M. Vanderhaeghen, P. Vernin
DAPNIA-SPhN, CE Saclay, France

J.Berthot, P.Y. Bertin, V. Breton, H. Fonvielle, Ch. Hyde-Wright[1)], G. Quemener, O. Ravel, Y. Roblin
LPC, Univ. Blaise Pascal, IN2P3 Aubiere, France
1) from Old Dominium University, Virginia, U.S.A

J. van de Wiele
IPN, IN2P3 Orsay, France

N. Degrande, H. Holvoet, B. Lannoy, G. de Meyer, D. Ryckbosch, Luc Van Hoorebeke, R. Van de Vyver
University of Gent, Belgium

W.U. Boeglin[2)], R. Böhm, M. Distler, R. Edelhoff, J. Friedrich, J.M. Friedrich, R. Geiges, P. Jennewein, M. Kahrau, M. Korn, H. Kramer, K.W. Krygier, V. Kunde, A. Liesenfeld, H. Merkel, K. Merle, R. Neuhausen, E.A.J.M. Offermann[3)], Th. Pospischil, G. Rosner, P.Sauer, H. Schmieden, S. Schardt, G. Tamas, A. Wagner, Th. Walcher*, S. Wolf
Institut für Kernphysik, Universität Mainz, Germany
2) from Florida International University, Florida, U.S.A
3) from CEBAF, VA, U.S.A

* *contact persons*

Abstract

We propose to study nucleon structure by Virtual Compton Scattering using the reaction $p(e,e'p)\gamma$ with the MAMI facility. We will detect the scattered electron and the recoil proton in coincidence in the high resolution spectrometers of the hall A1. Compton events will be separated from the other channels (principally π^0 production) by missing-mass reconstruction. We plan to investigate this reaction near threshold. Our goal is to measure new electromagnetic observables which generalize the usual magnetic and electric polarizabilities.

1 Introduction

One of the basic problems is the structure of nucleons in term of quarks and gluons. Despite many efforts, the non-perturbative structure of QCD has not yet been understood and it is clear that new experimental data are needed to guide the theoretical approaches, to exclude some scenarios or to constrain the models.

To be useful, the output of the experiment must be amenable to a simple interpretation in terms of elementary degrees of freedom. This is why purely electromagnetic processes are privileged tools since they can be interpreted directly in terms of the current carried by the quarks. In this respect, Virtual Compton Scattering (which can be accessed through the reaction $e + p \to e' + p' + \gamma$) is potentially a powerful tool to access nucleon structure. It is the natural complement to form factors, real Compton scattering and deep inelastic scattering.

In this reaction, the final photon can be emitted either by the electron or by the proton. The first process is described by Bethe-Heitler (BH) amplitude which is calculable from Quantum Electro-Dynamics (QED). The second process is described by the Full Virtual Compton Scattering ($FVCS$) amplitude which, in the one photon exchange approximation, is a linear combination of VCS amplitudes. Assuming that the one photon exchange approximation is valid, the BH and $FVCS$ amplitudes correspond to the graphs shown in Fig 1.

In this experiment we consider the kinematical regime defined by a center of mass (CM) energy ($\sqrt{s}$) of the final photon-proton system close to threshold. In particular we always assume that $\sqrt{s}$ is below the pion photoproduction threshold

$$m \leq \sqrt{s} \leq m + m_\pi$$

where m is the proton mass and m_π the pion mass.

The interest of the low energy regime (with arbitrary Q^2), is that it allows to measure new electromagnetic observables which generalize the usual magnetic and electric polarizabilities. These observables are clean probes of the non perturbative structure of the nucleon and are complementary to the elastic form factors. By contrast with the latter, the polarizabilities are controlled by the excitation spectrum of the QCD hamiltonian but, because of the threshold condition, the excited states contribute virtually. This is an advantage over real resonance production for which meson production and rescattering are the dominant process and must be treated explicitly even though they are not the interesting part of the problem in so far as nucleon structure is concerned. Below the pion production threshold, the situation is simpler because the excited states can not decay and therefore have no width, which is the hypothesis of most theoretical models of nucleon structure. This advantage is similar to the Deep Inelastic Scattering (DIS) regime for which it makes sense to use the parton model because the partons fragmentation can be neglected.

No data exist up to now for the $e + p \to e' + p' + \gamma$ reaction. Only real Compton scattering has been investigated so far in the low energy limit, on the proton at Moscow [1], Illinois [2], Mainz [3], Saskatoon [4] and on the neutron at Harwell [5] and Munich [6].

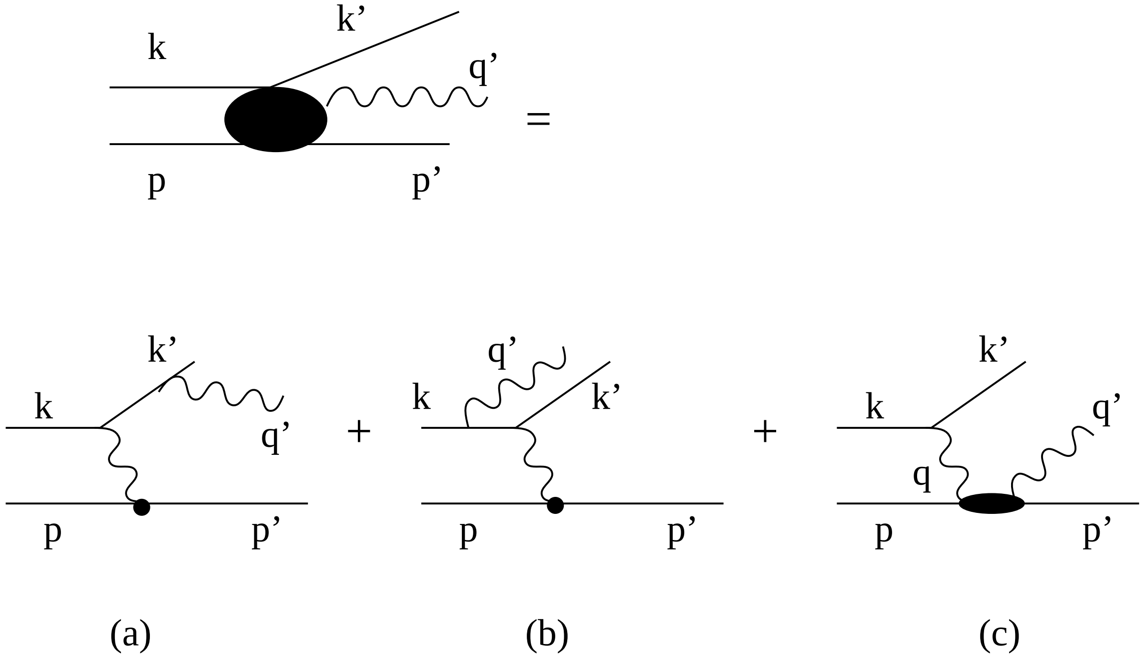

Figure 1: *The $p(e,e'p)\gamma$ reaction. The initial, final electron and initial, final proton quadri-momenta are k, k' and p, p' respectively. The final photon quadri-momentum is q'. a) and b) correspond to the Bethe-Heiler (BH) process. c) corresponds to the Full Virtual Compton Scattering (FVCS) process. We note q the quadri-momentum of the virtual photon exchanged in the FVCS process, that is $q = k - k'$.*

The low energy data, together with the dispersion relations have been used to determine the static electric and magnetic polarizabilities of the proton.

The polarizabitities (obtained in the low energy regime $\sqrt{s} \leq m + m_\pi$) are function only of Q^2, so it is interesting to investigate different domains in Q^2. The photon electroproduction experiments require a high duty cycle, so they are feasible at MAMI and at CEBAF. An experiment PR 93 050 is already accepted at CEBAF and has been scheduled in the range of Q^2 between 1 and 3 GeV^2 during the year 1996. The experiment at MAMI will give complementary measure at smaller Q^2 (from .15 to .35 GeV^2).

We propose to study the virgin field of photon electroproduction at MAMI by detecting the scattered electron and the recoil proton in coincidence in the high resolution spectrometers of the hall A1. We will benefit from the large duty cycle and the confortable luminosity ($\pounds \geq 10^{37}\mathrm{cm}^{-2}\mathrm{s}^{-1}$) provided by the Mainz facility. From the measured momenta of the scattered electron, recoil proton, and the incident beam energy, we reconstruct the missing mass m_X. The $e + p \to e' + p' + \gamma$ events are characterized by the photon mass : $m_X = 0$. Due to the CM to laboratory Lorentz boost, the outgoing proton momentum tends to be focused in a small cone around the virtual photon momentum. Thus a large phase space for the real photon is accessible in a single measurement of a coincidence between the scattered electron and the recoil proton detected in two spectrometers, despite the small solid angles.

The section 2 is an introduction of the appropriate formalism to analyze this threshold experiment and extract the “generalized polarizabilities” of the proton. The section 3 will explain how the experiment is planed, and will give the counting rates for the different kinematical conditions.

2 Theoretical aspects

In reference [7], the formalism appropriate to extract the “generalized polarizabilities” from photon electroproduction cross section is extensively developed. We only report the essential points.

In the photon electroproduction reaction off the proton

$$\begin{array}{ccccccccc} e & + & p & \to & e' & + & p' & + & \gamma \\ (k) & & (p) & & (k') & & (p') & & (q') \end{array}$$

we note (k, h), (k', h'), (q', λ') (quadri-momenta, helicity) of the initial electron, final electron, final photon respectively and (p, σ), (p', σ') (quadri-momenta, spin) of the initial proton and final proton respectively [1]. The heliticity is conserved ($h = h'$) as the electron

---

[1] We denote a quadri-momentum by k, an energy by k^0, a momentum vector by $\vec{k}$, a momentum modulus by $\mathbf{k}$.

mass can be neglected. We define q as the quadri-momentum of the virtual photon exchanged in the FVCS process, that is $q = k - k'$. We note θ (or $\theta^{\gamma\gamma}$) the angle between the final real photon and the initial virtual photon, $\theta^{\gamma p}$ the angle between the outgoing proton and the virtual photon, θ_e, θ_p, $\theta_{\gamma^{virtual}}$ the angles respectively of the scattered electron, the outgoing proton, the virtual photon comparatively to the initial electron, and φ the angle between the electron plane defined by $(\vec{k}, \vec{q})$ and the hadron plane defined by $(\vec{q'}, \vec{q})$. Since we are interested in the threshold region, it is quite natural to work in the CM frame. The variables in the CM frame will be defined without indices, and with the index *lab* in the laboratory system. The invariant quantities are :

$$Q^2 = -q^2, t = (q - q')^2, s = (p' + q')^2$$

The cross section has the form

$$\frac{d^5\sigma}{d\mathbf{k'}_{lab}[d\Omega_e]_{lab}[d\Omega_p]_{CM}} = \frac{(2\pi)^{-5}}{64m}\left(\frac{\mathbf{k'}_{lab}}{\mathbf{k}_{lab}}\right)\frac{s - m^2}{s} \times \mathcal{M}^{exp} \tag{1}$$

$\mathcal{M}^{exp}$ is invariant under a Lorentz transformation and is a function of the following center of mass variables :

- $\mathbf{q'}$: modulus of the momentum of the real photon
- $\mathbf{q}$: modulus of the momentum of the virtual photon
- θ : angle between the two photons
- ϵ : the rate of linear polarization of the virtual photon
- φ : the azimuthal angle of the electron plane versus the hadron plane.

The last two variables are the same in the *lab* and CM frame. The amplitude for the VCS are functions of the variable $(\mathbf{q}, \mathbf{q'}, \theta)$ which are directly connected to the invariants (Q, s, t). The variables ϵ and φ are related to the lepton kinematics and will be present in the expression of the $FVCS$ and BH processes.

The probability $\mathcal{M}^{exp}$ is a coherent sum of two matrix element,

$$\mathcal{M}^{exp} = \frac{1}{4}\sum_{\sigma\sigma'h'\lambda'}|T^{ee'\gamma}|^2 = \frac{1}{4}\sum_{\sigma\sigma'h'\lambda'}|T^{BH} + T^{FVCS}|^2 \tag{2}$$

where T^{BH} and T^{FVCS} are respectively the matrix elements for the Bethe Heitler (BH) and Full Virtual Compton Scattering (FVCS) processes. In the one photon exchange approximation, one has :

$$T^{FVCS} = \frac{-e^3}{Q^2}\sum_{\lambda}\Omega(h, \lambda)T^{VCS}(\lambda', \lambda)$$

where λ is the virtual photon helicity, T^{VCS} is the Virtual Compton Scattering off the proton and $\Omega(h, \lambda)$ the lepton current. One writes :

$$T^{VCS} = T^N + R$$

where T^N is the nucleon contribution and R is the contribution of the higher energy states. These latter start at $\sqrt{s} = m + m_\pi$ which garanties that the energy denominators do not vanish at the soft photon point. So the sum R over all the possible states except the nucleon, is regular.

For gauge invariance consideration, one separates the Born term T^{Born} (see precisely the definition of this Born term in the reference [7]) in the VCS matrix element :

$$T^{VCS} = T^{Born} + (T^N - T^{Born}) + R$$

We note : $$T^{NonBorn} = (T^N - T^{Born}) + R = T^{VCS} - T^{Born}.$$

In an expansion in powers of **q**', the first terms of the amplitudes T^{BH} and T^{Born} are of order $\mathbf{q}'^{-1}$, while the first term of $T^{NonBorn}$ is of order $\mathbf{q}'$ according to Low's theorem [8]. So one can write :

$$T^{ee'\gamma} = \underbrace{T^{BH} + \frac{-e^3}{Q^2}\sum \Omega . T^{Born}}_{\alpha_{-1}\mathbf{q}'^{-1}+\alpha_0\mathbf{q}'^{0}+\alpha_1\mathbf{q}'+0(\mathbf{q}'^2)} + \underbrace{\frac{-e^3}{Q^2}\sum \Omega . T^{NonBorn}}_{\frac{-e^3}{Q^2}\sum\Omega.(\beta_1\mathbf{q}'+0(\mathbf{q}'^2))} \tag{3}$$

where $\alpha_{-1}, \alpha_0, \alpha_1$ are known functions of the kinematical variables $(\mathbf{q}, \epsilon, \theta, \varphi)$.
T^{BH} and T^{Born} are completly calculable once the elastic form factors of the proton are known.

The term β_1 which is $[T^{NonBorn}/\mathbf{q}']_{\mathbf{q}'=0}$ is proton structure dependent and can be parametrized by 10 real functions of Q^2 or $\mathbf{q}$ (at $\mathbf{q}' = 0$, we have $Q^2 = -2m^2 + 2m\sqrt{m^2+\mathbf{q}^2}$). The coefficients of the parametrisation contain the dependence in the variables $(\mathbf{q}, \epsilon, \theta, \varphi)$. The 10 functions are distinguished by the spin flip or non spin flip character of the reaction and by the total angular momentum of the photons. In the Non Born term which is linear in $\mathbf{q}'$ the final photon can only be dipole electric or magnetic while for finite Q^2 the initial photon is only restricted by parity and angular momentum conservation. The selection rules used to determine the number of these functions originate from parity and total angular momentum conservation as expressed in equations :

$$(-1)^{\rho+L} = (-1)^{\rho'+L'} \qquad \rho, \rho' = 0, 1, 2$$

$$|L - L'| \leq S \leq L + L' \qquad S = 0, 1$$

The index ρ (resp. ρ') refers to the electric (2), magnetic (1) and longitudinal (0) character of the initial (resp. final) photon. L is the total angular momentum of the initial photon (L'=1 for the final photon) and S refer to the spin (S=1) and non spin-flip (S=0) character of the transition. The table 1 presents the possible quantum numbers of these functions $\beta_1^{(\rho'L',\rho L)S}$.

To parametrize these 10 functions, one needs 10 "generalized polarizabilities" :

$$P^{(11,00)1}, P^{(11,02)1}, P^{(11,11)0}, P^{(11,11)1}, \hat{P}^{(11,2)1}$$

$$P^{(01,01)0}, P^{(01,01)1}, P^{(01,12)1}, \hat{P}^{(01,1)0}, \hat{P}^{(01,1)1}$$

which have been defined in such a way that their limit at $\mathbf{q} \to 0$ is the same as the real photon limit (we note $\tilde{q}_0$ the energy of the virtual photon at $\mathbf{q}' = 0$ ($\tilde{q}_0 = m - \sqrt{m^2+\mathbf{q}^2} \overset{\mathbf{q}\to 0}{\to} \frac{\mathbf{q}^2}{2m}$). The parametrization is :

Polarizabilities					
ρ'	ρ	**L**	**S**	**Multipole** $(\gamma^{real}, \gamma^{virtual})$	**notation** $\beta_1^{(\rho' L', \rho L)S}$
1	0	0,2	1	$(M1, L0), (M1, L2)$	$\beta_1^{(11,00)1}, \beta_1^{(11,02)1}$
	2	2	1	$(M1, E2)$	$\beta_1^{(11,22)1}$
	1	1	0,1	$(M1, M1)$	$\beta_1^{(11,11)0}, \beta_1^{(11,11)1}$
2	0	1	0,1	$(E1, L1)$	$\beta_1^{(21,01)0}, \beta_1^{(21,01)1}$
	2	1	0,1	$(E1, E1)$	$\beta_1^{(21,21)0}, \beta_1^{(21,21)1}$
	1	2	1	$(E1, M2)$	$\beta_1^{(21,12)1}$

Table 1: *Conventions for the notation of the involved multipoles. The index ρ (resp. ρ') refers to the electric (2), magnetic (1) and longitudinal (0) character of the initial (resp. final) photon. L is the total angular momentum of the initial photon (L'=1 for the final photon) and S refers to the spin (S=1) and non spin-flip (S=0) character of the transition.*

$$\beta_1^{(11,\rho L)S}(\mathbf{q}) = \mathbf{q}^L \, P^{(11,\rho L)S}(\mathbf{q}) \qquad (\rho = 0,1)$$

$$\beta_1^{(11,2L)S}(\mathbf{q}) = -\mathbf{q}^L \, \left[\sqrt{\frac{L+1}{L}} \frac{\tilde{q}_0}{\mathbf{q}} P^{(11,0L)S}(\mathbf{q}) + \mathbf{q} \sqrt{\frac{2L+1}{L}} \hat{P}^{(11,L)S}(\mathbf{q}) \right]$$

$$\beta_1^{(21,\rho L)S}(\mathbf{q}) = -\mathbf{q}^L \sqrt{2} P^{(01,\rho L)S}(\mathbf{q}) \qquad (\rho = 0,1)$$

$$\beta_1^{(21,2L)S}(\mathbf{q}) = \mathbf{q}^L \, \sqrt{2} \, \left[\sqrt{\frac{L+1}{L}} \frac{\tilde{q}_0}{\mathbf{q}} P^{(01,0L)S}(\mathbf{q}) + \mathbf{q} \sqrt{\frac{2L+1}{L}} \hat{P}^{(01,L)S}(\mathbf{q}) \right]$$

As an illustration, equations 4 and 5 give the "generalized polarizabilities" in two important cases :

$$\begin{aligned} P^{(01,01)0}(\mathbf{q}) = \sqrt{\frac{2}{3}} \quad & \Sigma_{(X \neq N)} [< N|d(0)|X >< X|d(\mathbf{q})|N > \\ & + < N|d(\mathbf{q})|X >< X|d(0)|N >] \, \tfrac{1}{m - m_X} \end{aligned} \tag{4}$$

$$d(\mathbf{q}) = \int d\vec{r} \frac{3 j_1(\mathbf{q} r)}{\mathbf{q} r} J^0(\vec{r}) z$$

$$\begin{aligned} P^{(11,11)0}(\mathbf{q}) = \frac{4}{\sqrt{6}} \quad & \Sigma_{(X \neq N)} [< N|\mu(0)|X >< X|\mu(\mathbf{q})|N > \\ & + < N|\mu(\mathbf{q})|X >< X|\mu(0)|N >] \, \tfrac{1}{m - m_X} \end{aligned} \tag{5}$$

$$\mu(\mathbf{q}) = \frac{1}{2} \int d\vec{r} \frac{3j_1(\mathbf{q}r)}{\mathbf{q}r} \left[\vec{r} \times \vec{J}\right]_z$$

where J^μ is the hadronic current. When $\mathbf{q} \to 0$, $[3j_1(\mathbf{q}r)/\mathbf{q}r] \to 1$ so that, up to a constant factor, we recognize in equations (4, 5) the usual electric (α) and magnetic (β) polarizabilities of the nucleon. Explicitly :

$$P^{(01,01)0}(0) = -\sqrt{\frac{2}{3}\frac{\alpha}{e^2}} \quad ; \quad P^{(11,11)0}(0) = -\sqrt{\frac{8}{3}\frac{\beta}{e^2}}$$

It should be clear that the measurement of these "generalized polarizabilities" through Virtual Compton Scattering will enlarge enormously the set of electromagnetic observables against which the nucleon structure models can be compared.

We assume (see eqs 2,3) that at fixed $(\mathbf{q}, \epsilon, \theta, \varphi)$ the experiment near threshold ($\mathbf{q}' \leq m_\pi$) determines $\mathcal{M}^{exp}$ (equation 6) in the form :

$$\mathcal{M}^{exp} = \frac{\mathcal{M}^{exp}_{-2}}{\mathbf{q}'^2} + \frac{\mathcal{M}^{exp}_{-1}}{\mathbf{q}'} + \mathcal{M}^{exp}_0 + 0(\mathbf{q}') \tag{6}$$

where the coefficients $\mathcal{M}^{exp}_i$, i=-2,-1,0 are functions of $(\mathbf{q}, \epsilon, \theta, \varphi)$.

One defines (see ref. [7]) :

$$\frac{1}{4} \sum_{spin} |T^{BH} + T^{Born}|^2 = \frac{\mathcal{M}^{LET}_{-2}}{\mathbf{q}'^2} + \frac{\mathcal{M}^{LET}_{-1}}{\mathbf{q}'} + \mathcal{M}^{LET}_0 + 0(\mathbf{q}') \tag{7}$$

The coefficients $\mathcal{M}^{LET}_i$, i=-2,-1,0 are calculable functions of $(\mathbf{q}, \epsilon, \theta, \varphi)$. The best is to do it numerically because it is easier to compute $(T^{BH} + T^{Born})$ at a given kinematical point and then make a fit on $\mathbf{q}'$ than to calculate analytically the developpement of equation (7).

The first ouput of the experiment is a test of the low energy theorem in the form :

$$\begin{aligned} \mathcal{M}^{exp}_{-2}(\mathbf{q}, \epsilon, \theta, \varphi) &= \mathcal{M}^{LET}_{-2}(\mathbf{q}, \epsilon, \theta, \varphi) & (8) \\ \mathcal{M}^{exp}_{-1}(\mathbf{q}, \epsilon, \theta, \varphi) &= \mathcal{M}^{LET}_{-1}(\mathbf{q}, \epsilon, \theta, \varphi) & (9) \end{aligned}$$

This is a crucial part of the experiment because it will validate the expansion assumed in equation (6).

Then, in a second step, $\mathcal{M}^{exp}_0 - \mathcal{M}^{LET}_0$ will give a linear system for the "generalized polarizabilities". This term is the product of the coefficients α_{-1} and β_1 in equation 3. This is an **interference** between the term of order $\mathbf{q}'^{-1}$ of $(T^{BH} + T^{Born})$ and the term of order $\mathbf{q}'$ in $T^{NonBorn}$, which is parametrized by the 10 "generalized polarizabilities". In the case of unpolarized experiment one gets (see ref.[7]) :

$$
\begin{aligned}
\mathcal{M}_0^{exp} - \mathcal{M}_0^{LET} = {} & \frac{4me^6\mathbf{q}}{\tilde{Q}^2(1-\epsilon)}\sqrt{\frac{2E(\mathbf{q})}{E(\mathbf{q})+m}} \\
& \{ sin\theta \left(\omega'' sin\theta - \omega' \mathbf{k}_T cos\varphi cos\theta\right) \left(\epsilon P_{LL}(\mathbf{q}) - P_{TT}(\mathbf{q})\right) \\
& - \left(\omega'' sin\theta cos\varphi - \omega' \mathbf{k}_T cos\theta\right) \sqrt{2\epsilon(1+\epsilon)} P_{LT}(\mathbf{q}) \\
& - \left(\omega'' sin\theta cos\theta cos\varphi - \omega' \mathbf{k}_T (1 - cos^2\varphi sin^2\theta)\right) \sqrt{2\epsilon(1+\epsilon)} P'_{LT}(\mathbf{q}) \Big\}
\end{aligned}
\tag{10}
$$

The variables $\tilde{Q}, \mathbf{k}_T, \omega, \omega', \omega''$ and $E(\mathbf{q})$ present in expression (10) are the kinematical variables when the real photon energy is zero (which is equivalent to take the variables at the elastic scattering condition) :

$$
\begin{aligned}
\tilde{Q} &= [Q]_{\mathbf{q}'=0} \\
\mathbf{k}_T &= \tilde{Q}\sqrt{\frac{\epsilon}{2(1-\epsilon)}} \\
\omega &= -\left[\mathbf{q}'\left(\frac{1}{p.q'} + \frac{1}{k.q'}\right)\right]_{\mathbf{q}'=0} \\
\omega' &= +\left[\mathbf{q}'\left(\frac{1}{k'.q'} - \frac{1}{k.q'}\right)\right]_{\mathbf{q}'=0} \\
\omega'' &= +\left[\omega\mathbf{q} - \omega'\sqrt{\mathbf{k}'^2 - \mathbf{k}_T{}^2}\right]_{\mathbf{q}'=0} \\
E(\mathbf{q}) &= \sqrt{\mathbf{q}^2 + m^2}
\end{aligned}
$$

The amplitudes P_{LL}, P_{TT}, P_{LT} and P'_{LT} are the following combination of "generalized polarizabilities" :

$$
\begin{aligned}
P_{LL}(\mathbf{q}) = {} & -2\sqrt{6} m G_E(\tilde{Q}) P^{(01,01)0}(\mathbf{q}) \\
P_{TT}(\mathbf{q}) = {} & \frac{3}{2} G_M(\tilde{Q}) \left(2\tilde{q}_0 P^{(01,01)1}(\mathbf{q}) + \sqrt{2}\mathbf{q}^2(\sqrt{3}\hat{P}^{(01,1)1}(\mathbf{q}) + P^{(01,12)1}(\mathbf{q})\right) \\
P_{LT}(\mathbf{q}) = {} & \sqrt{\frac{3}{2}} m \frac{\mathbf{q}}{\tilde{Q}} G_E(\tilde{Q}) P^{(11,11)0}(\mathbf{q}) + \frac{\sqrt{3}\tilde{Q}}{2\mathbf{q}} G_M(\tilde{Q}) \left(P^{(11,00)1}(\mathbf{q}) + \frac{\mathbf{q}^2}{\sqrt{2}} P^{(11,02)1}(\mathbf{q})\right) \\
P'_{LT}(\mathbf{q}) = {} & \sqrt{\frac{3}{2}} \frac{m}{\tilde{Q}} G_E(\tilde{Q}) \left(2\tilde{q}_0 P^{(01,01)0}(\mathbf{q}) + \sqrt{6}\mathbf{q}^2 \hat{P}^{(01,1)0}(\mathbf{q})\right) - \frac{3}{2}\tilde{Q} G_M(\tilde{Q}) P^{(01,01)1}(\mathbf{q})
\end{aligned}
$$

The second step of the analysis will then be carried out in the following way :

- In order to extract the three combinations $(\epsilon P_{LL}(\mathbf{q}) - P_{TT}(\mathbf{q}))$, $P_{LT}(\mathbf{q})$ and $P'_{LT}(\mathbf{q})$ from the equation 10, we have to play at fixed $\mathbf{q}$ and ϵ with different sets (θ, φ) in order to vary the interference between the Bethe-Heitler and the FVCS terms.

- The separation of $P_{LL}(\mathbf{q})$, $P_{TT}(\mathbf{q})$ implies an experiment with at least two different values of ϵ. The interest of $P_{LL}(\mathbf{q})$ is that it is proportional to $P^{(01,01)0}(\mathbf{q})$ which has for limit when $(\mathbf{q}) \to 0$, the usual electric polarizabity α of the nucleon.

Figures 2 and 3 represent the three contributions to the cross sections of respectively $|T^{BH}|^2$, $|T^{Born}|^2$, and $|T^{BH} + T^{Born}|^2$ as a function of $\theta_{lab}^{\gamma\gamma}$ for 2 different values of φ in the domain studied at MAMI ($\mathbf{q}$ = 600 MeV, $\mathbf{q}'$ = 67.5 MeV, $\epsilon = 0.62$). As it is well known the BH process is strongly peaked along the electron lines. This allows us to define regions in (θ, φ) for the final photon where BH is either dominant, or comparable to the $FVCS$ thereby favouring the interference (in this figure only the Born contribution is taken into account).

An important question about the determination of the "generalized polarizabilities" (from the formule 10) is whether the deviation from the low energy theorem is large enough below the pion threshold to be measured accurately. To this aim, a first estimate of the "generalized polarizabilities" has been done in the Non Relativistic Quark Constituant Model [7]. The two contributions $|T^{BH}+T^{Born}|^2$ and $|T^{BH}+T^{Born}+T^{NonBorn}|^2$ (calculated in the NRQCM) are indicated respectively in figure 4 in a logarithmic scale and in figure 5 in a linear scale which is a zoom of the promising region ($\theta_{CM}^{\gamma\gamma}$ from $-180°$ to $0°$). The deviation $(\sigma_{BH+Born+\Delta} - \sigma_{BH+Born})/\sigma_{BH+Born}$ shown in figure 6 is rather damped in the region around the initial and scattered electron directions, but outside reaches a maximum of 13%. This estimation is also presented in figure 7 which illustrates the experiment method. The deviation from the LET predicted for $\mathbf{q'}^2 \times \mathcal{M}^{exp}$ (refer to equation 6) at fixed $(\mathbf{q}, \epsilon, \theta, \varphi)$ in the NRQCM is a sizable effect which we should be able to measure. This supports the idea that a fruitful study of the Virtual Compton Scattering in the low energy regime is possible.

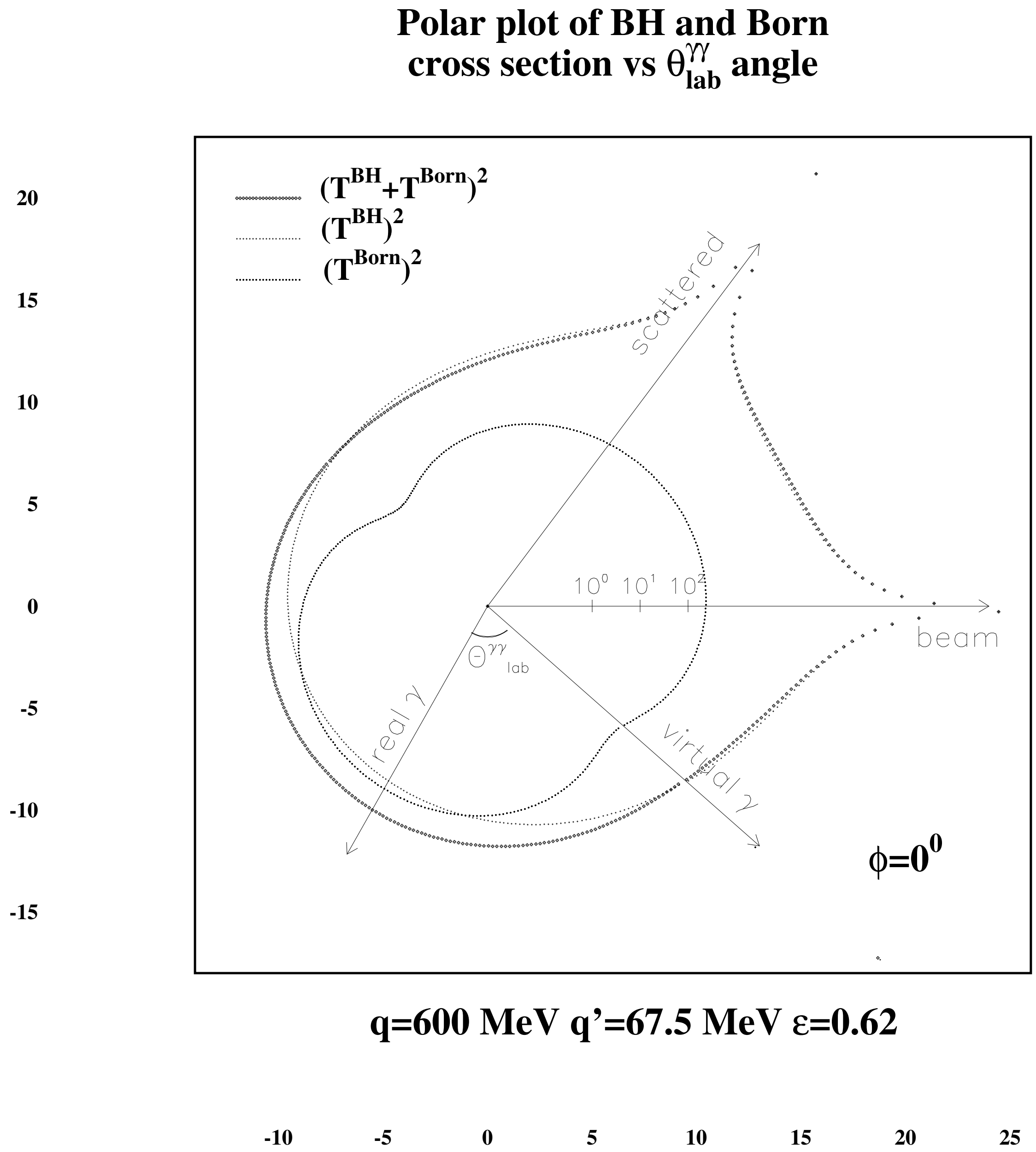

Figure 2: *The three contributions to the cross sections respectively for* $|T^{BH}|^2$, $|T^{Born}|^2$, *and the coherent sum* $|T^{BH}+T^{Born}|^2$ *as a function of* $\theta^{\gamma\gamma}_{lab}$ *for 2 different values of* φ *(*$0°$ *and* $60°$*) in a typical domain studied at MAMI (*$\boldsymbol{q} = 600$ *MeV,* $\boldsymbol{q}' = 67.5$ *MeV,* $\epsilon = 0.62$*). For given (*$\boldsymbol{q}$*,* $\boldsymbol{q}'$*,* ϵ*), the incident electron, scattered electron and virtual photon directions are completly defined. At* $\varphi = 0°$*, these 3 axes are indicated. As* $\theta^{\gamma\gamma}_{lab}$ *varies from* $-180°$ *to* $180°$*, the real photon direction turns around the virtual photon direction. The cross sections (in pb/GeV sr2) are reported in a logarithmic scale on each radius corresponding to the direction of the real photon.*

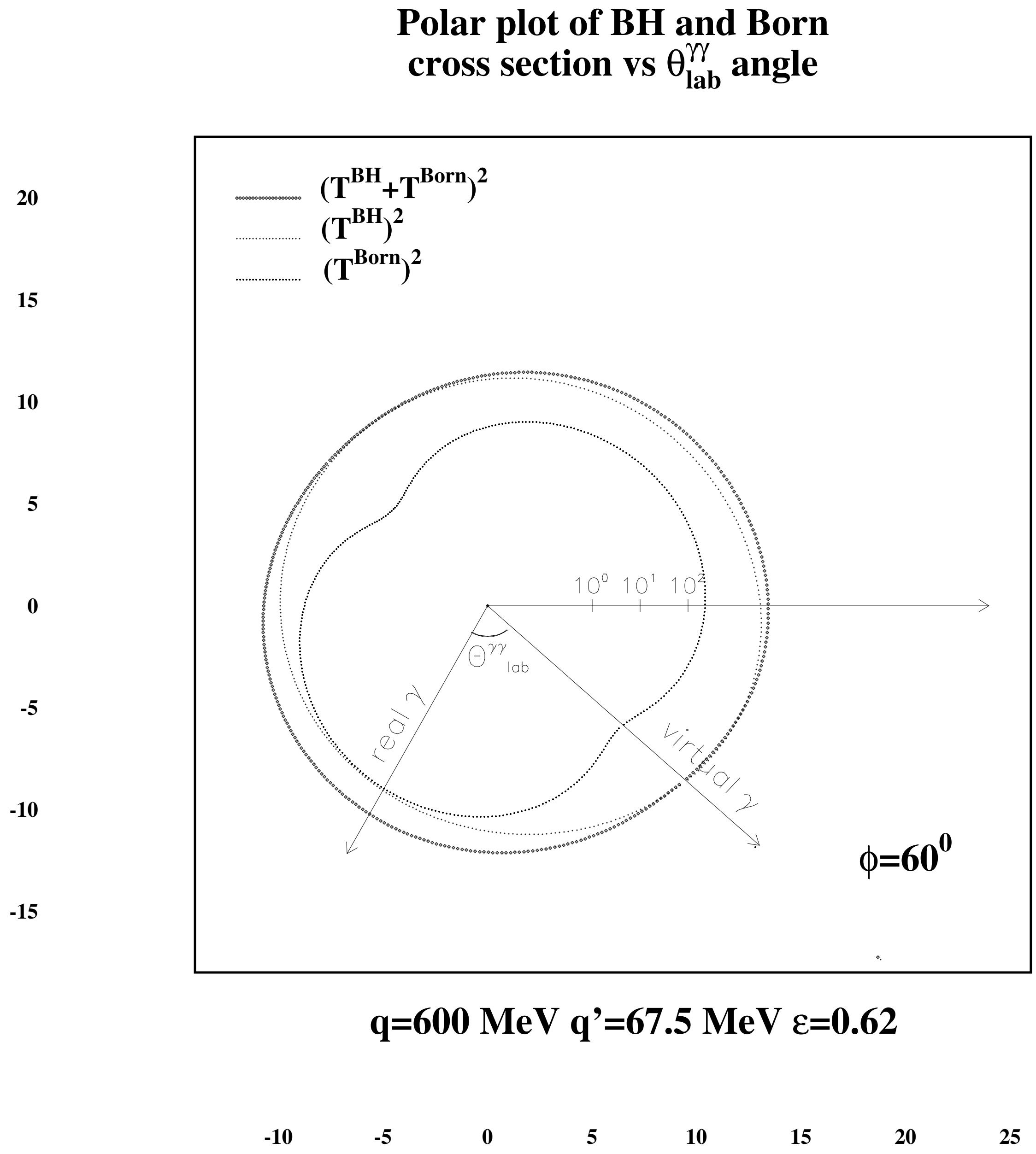

Figure 3: *The three contributions to the cross sections respectively for* $|T^{BH}|^2$, $|T^{Born}|^2$, *and the coherent sum* $|T^{BH}+T^{Born}|^2$ *as a function of* $\theta^{\gamma\gamma}_{lab}$ *for 2 different values of* φ *(*0° *and* 60°*) in a typical domain studied at MAMI (*$\boldsymbol{q}$ = 600 *MeV*, $\boldsymbol{q'}$ = 67.5 *MeV*, $\epsilon = 0.62$*). For given (*$\boldsymbol{q}$, $\boldsymbol{q'}$, ϵ*), the incident electron, scattered electron and virtual photon directions are completly defined. At* $\varphi = 60^\circ$, *only the virtual photon axis is present. As* $\theta^{\gamma\gamma}_{lab}$ *varies from* -180° *to* 180°, *the real photon direction turns around the virtual photon direction. The cross sections (in pb/GeV sr2) are reported in a logarithmic scale on each radius corresponding to the direction of the real photon.*

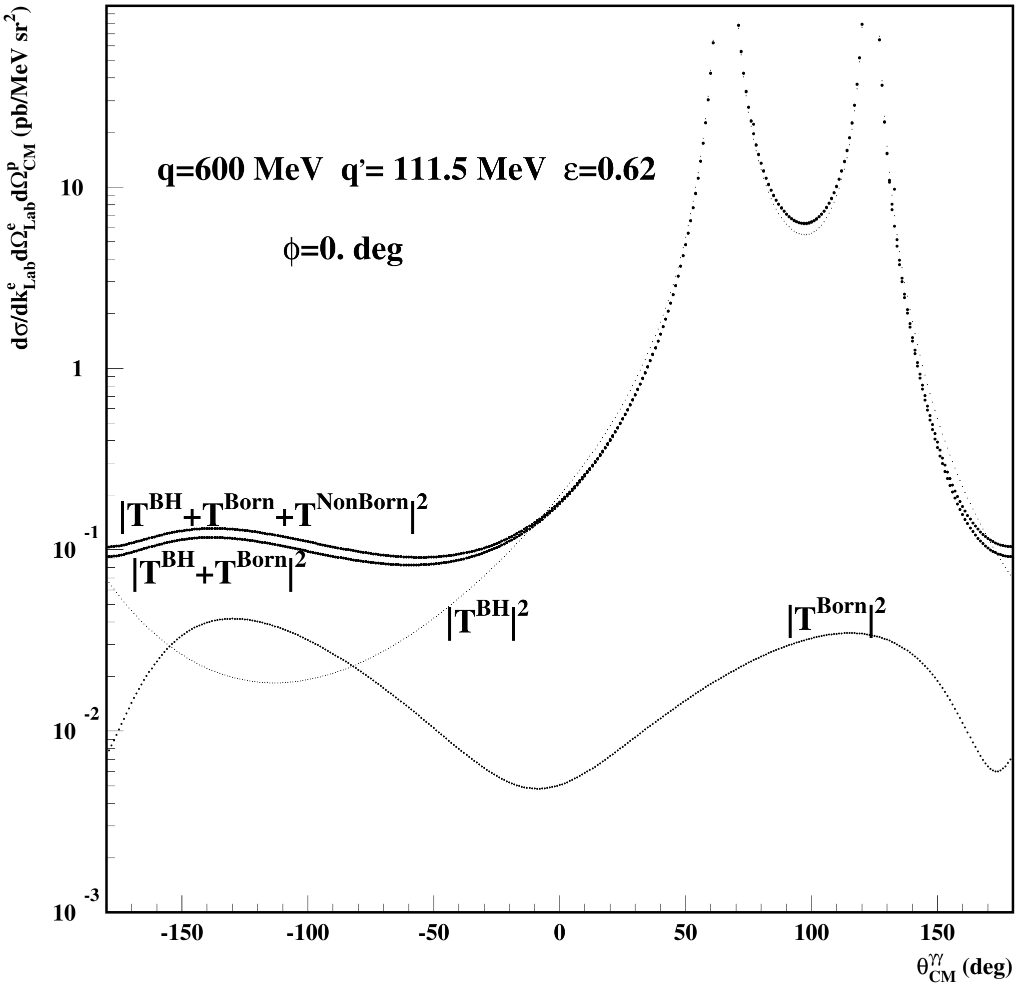

Figure 4: *The two contributions* $|T^{BH} + T^{Born}|^2$ *and* $|T^{BH} + T^{Born} + T^{NonBorn}|^2$ *are indicated in a logarithmic scale as a function of* $\theta^{\gamma\gamma}_{CM}$ *in the kinematical domain studied at MAMI (*$\boldsymbol{q}$ = 600 *MeV,* $\boldsymbol{q}'$ = 111.5 *MeV,* ϵ = 0.62*,* φ = 0°*). The "generalized polarizabilities" introduced in the Non Born term are estimated in the NRQCM.*

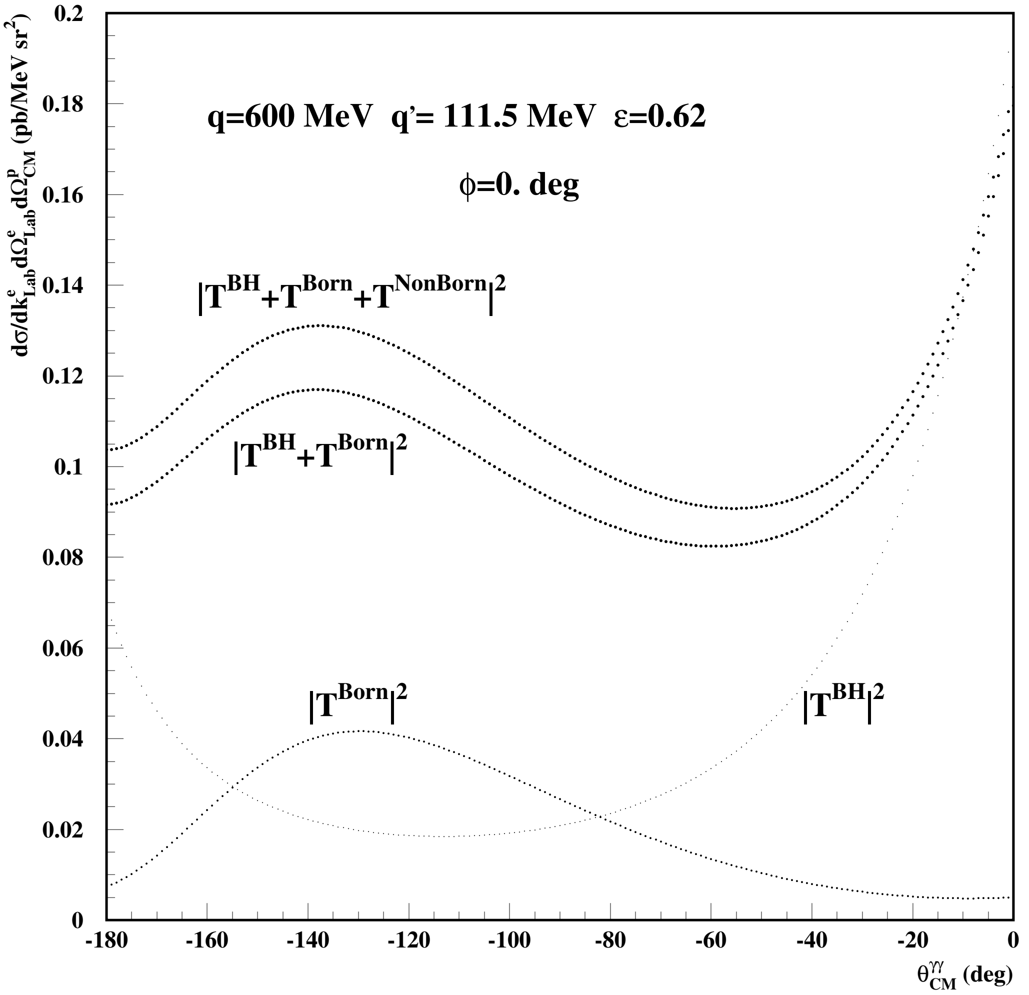

Figure 5: *Zoom of the previous figure : the two contributions* $|T^{BH}+T^{Born}|^2$ *and* $|T^{BH}+T^{Born}+T^{NonBorn}|^2$ *are indicated in a linear scale in the promising region of* $\theta^{\gamma\gamma}_{CM}$ *(from -180° to 0°) in the kinematical domain studied at MAMI (*$\boldsymbol{q}=600$ *MeV,* $\boldsymbol{q'}=111.5$ *MeV,* $\epsilon=0.62$*),* $\varphi=0°$*. The "generalized polarizabilities" introduced in the Non Born term are estimated in the NRQCM.*

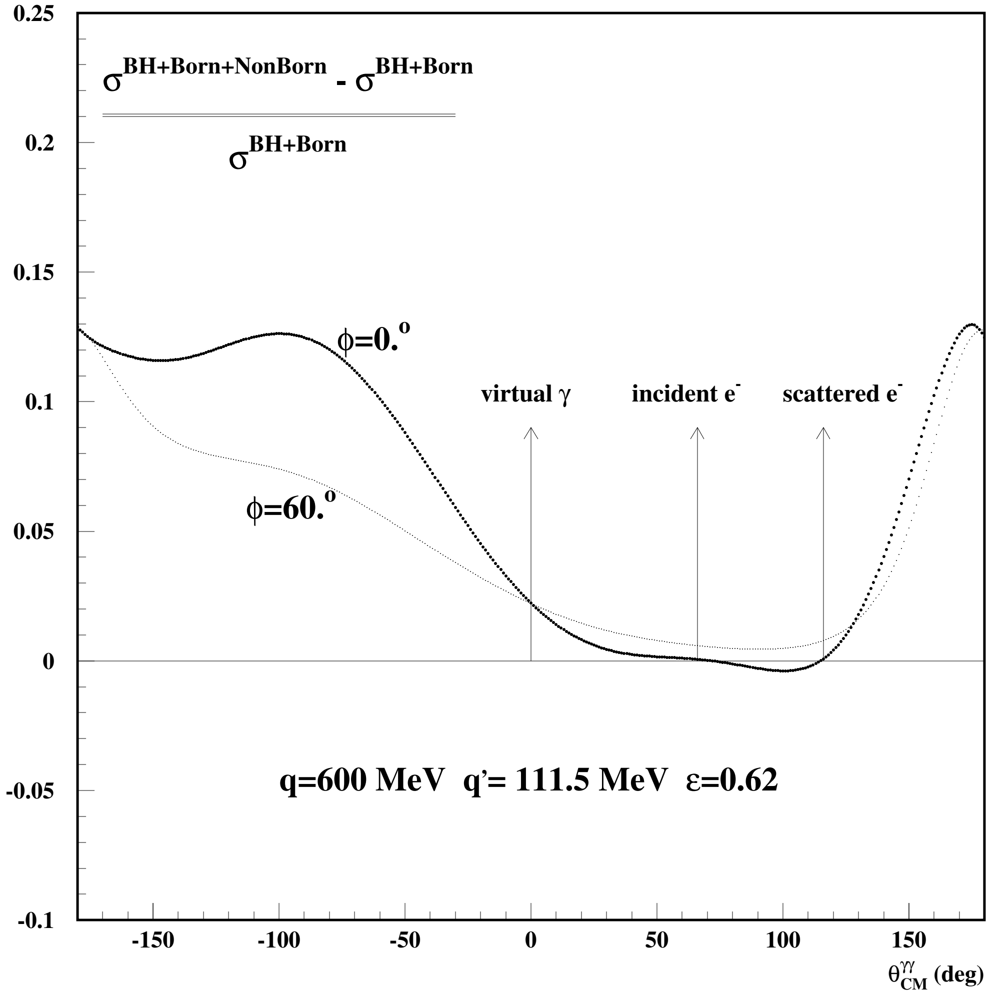

Figure 6: *Effect of the polarizabilities calculated in the NRQCM. The deviation* $(\sigma_{BH+Born+\Delta} - \sigma_{BH+Born})/\sigma_{BH+Born}$ *is a function of* $\theta^{\gamma\gamma}_{lab}$ *for 2 values of* φ $(0°$ *and* $60°)$ *at* $\boldsymbol{q'} = 111.5$ *MeV,* $\boldsymbol{q} = 600$ *MeV and* $\epsilon = 0.62$.

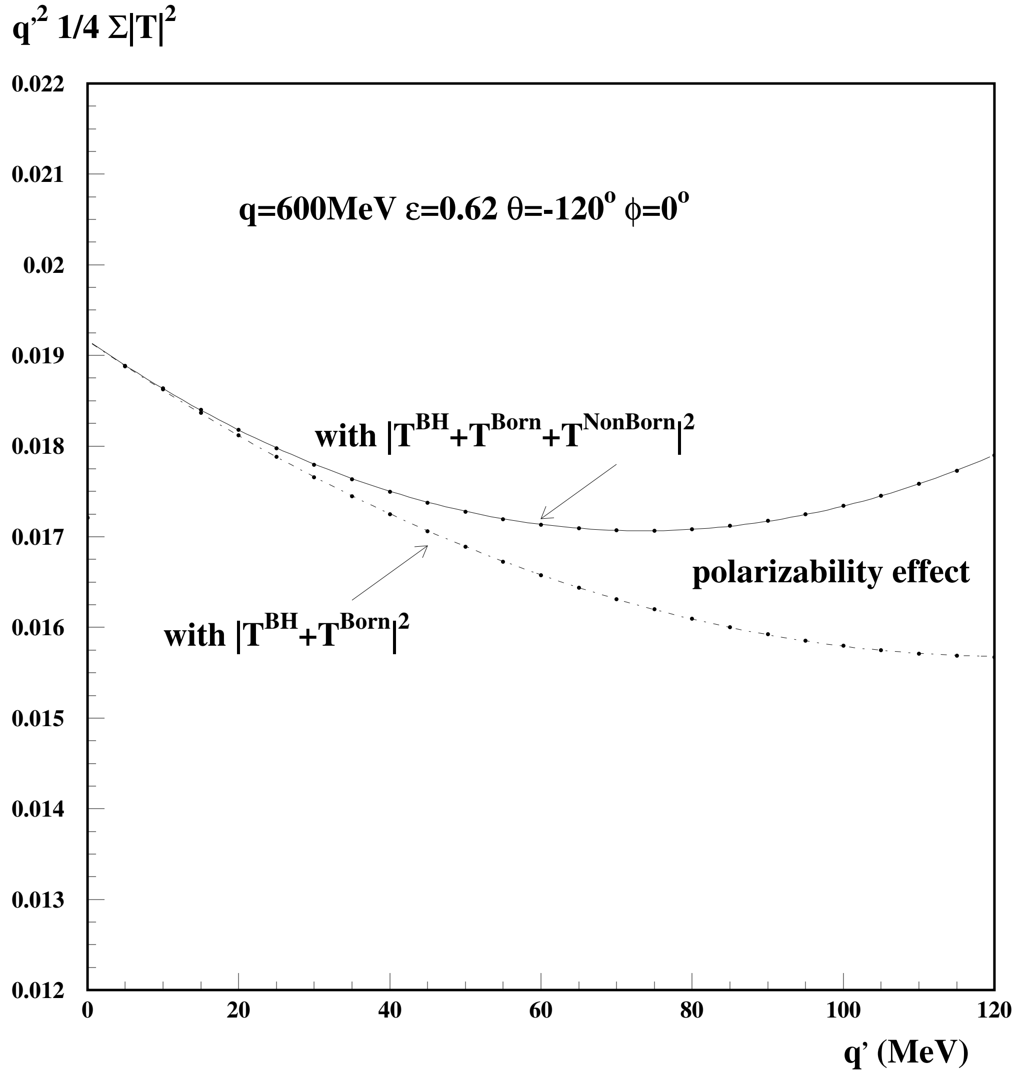

Figure 7: *The experimental method consists to study the evolution of* $\boldsymbol{q}'^2 \times \mathcal{M}^{exp}$ *(refer to equation (6)) at fixed* $(\boldsymbol{q}, \epsilon, \theta, \varphi)$. *In a polynomial fit, the parameter of the second order in* $\boldsymbol{q}'$ *will provide the LET prediction plus the polarizability effect.*

3 Experimental aspects

3.1 Choice of kinematics for the proposed study

Our goal is to measure the "generalized polarizabilities" according the analysis method presented in the previous section and which has the benefit to be model independant. We recall the relevant variables for the theoretical aspects :

$$(\mathbf{q}, \mathbf{q}', \epsilon, \theta, \varphi)$$

and we summarize their role. The polarizabilities are only function of $\mathbf{q}$, so for a first experiment we can choice judiciously a unique value of $\mathbf{q}$. In a first step of the analysis, we have to determine the domain of validity of the low energy theorem. We have to study the photon electroproduction cross section as a function of $\mathbf{q}'$ for fixed values of $(\mathbf{q}, \epsilon, \theta, \varphi)$ in order to perform a precise fit on an expansion in powers of $\mathbf{q}'$ (see formula (6)). It is necessary to investigate the low energy region under the pion photoproduction threshold for example at 5 values of $\mathbf{q}'$ $\underline{(\mathbf{q}' = 21.5, 45.0, 67.5, 90.0, 111.5 \text{ MeV})}$. Then, in a second step, our goal is to investigate this reaction in a large domain of (θ, φ) in order to obtain many combinations of the polarizabilities and to solve accurately the system (see formula (10)). It would be required at least two different values of ϵ to separate $P_{LL}(\mathbf{q})$ and $P_{TT}(\mathbf{q})$.

Experimentaly we study the reaction $e + p \to e' + p' + \gamma$ by detecting the scattered electron and recoil proton in coincidence in two high resolution spectrometers.

Due to the CM to *lab* Lorentz boost, the outgoing proton momentum tends to be focused in a small cone around the virtual photon momentum. Thus a large phase space for the real photon is accessible in a single measurement of a coincidence between the scattered electron and the recoil proton detected in two spectrometers, despite the small solid angles.

We measure 7 experimental observables, the incident beam energy, the momenta and angles of the scattered electron and of the recoil proton :

$$(\mathbf{k}_{lab}, \mathbf{k}'_{lab}, \mathbf{p}'_{lab}, \theta_{e_{lab}}, \theta_{p_{lab}}, \varphi_{e_{lab}}, \varphi_{p_{lab}})$$

With these quantities, we reconstruct the missing mass m_X^2. The $e + p \to e' + p' + \gamma$ events are characterized by the photon mass: $m_X^2 = 0$, which is clearly separated from the π^0 contribution at $m_X^2 = 0.0182$ GeV^2 thanks to the excellent energy resolution given by the facilities in Mainz (very good resolutions for beam and spectrometers).

The maximum energy of $\mathbf{k}_{lab}$, the electron beam is 0.855 GeV with a resolution $\Delta\mathbf{k}_{lab}/\mathbf{k}_{lab}$ better than 10^{-4}. With the high duty cycle, we are not limited by the accidental counting rates, and we can use the maximum luminosity. A luminosity $\mathcal{L} = 10^{37}$ cm^{-2} s^{-1} which will be used in the following evaluations, corresponds to a 20 μA beam current on a 2 cm length liquid hydrogen target. (We have consider a target cell with a vertical cylindrical wall made of 7.5 μm stainless steel.)

The main characteristics of the spectrometers A and B, are presented in table 2.

	A	**B**
maximum momentum (MeV/c)	735	870
momentum acceptance (%)	20	15
solid angle (msr)	21	5.6
horizontal acceptance (mrad)	± 75	± 20
vertical acceptance (mrad)	± 70	± 70
scattering angle range (deg)	18-160	7-62
length of central target	10.75	12.03
dispersion (cm/%)	5.77	8.22
momemtum resolution	$\leq 10^{-4}$	$\leq 10^{-4}$
length target acceptance (mm)	50	50
angular resolution at target (mrad)	≤ 3	≤ 3
position resolution at target (mm)	5	1

Table 2: *main characteristics of the two spectrometers A and B.*

The A spectrometer, of largest solid angle, is the best suited to detect the proton in order to collect the largest number of protons whose momenta describe a cone around the virtual photon momentum.

Moreover it is convenient to use the B spectrometer of smallest solid angle and horizontal acceptance to detect the electron since $(\mathbf{q}, \mathbf{q}', \epsilon)$, equivalent to $(\mathbf{k}_{lab}, \mathbf{k}'_{lab}, \theta_{e_{lab}})$, are expected to vary in a small range along the spectrometer acceptance in order to control the low energy theorem.

The lower limit of Q^2 accessible at MAMI ($Q^2 = 0.15$ GeV^2) is given by the minimum momemtum of a proton going out the target (250 MeV/c) ; the upper limit $Q^2 = 0.35$ GeV^2 is constrainted by the maximum energy of the electron beam, the angular and the momentum limits of the spectrometers. So the $\mathbf{q}$ resulting value (according the formula (11)) varies from 390 MeV to 660 MeV. The largest is $\mathbf{q}$, the more efficient is the Lorentz boost, which is of a crucial help in the experiment. In that first experiment, we propose to choose $\underline{\mathbf{q} = 600 \text{ MeV}}$.

3.1.1 Definition of the leptonic arm according to $\mathbf{q}, \mathbf{q}', \epsilon$

It exists a complete bijection between the 2 sets of variables $(\mathbf{q}, \mathbf{q}', \epsilon)$ and $(\mathbf{k}_{lab}, \mathbf{k}'_{lab}, \theta_{e_{lab}})$. We recall the main relations (when we neglect the electron mass before its momentum) :

$$\begin{aligned}
q^0_{lab} &= k^0_{lab} - k'^0_{lab} = \mathbf{k}_{lab} - \mathbf{k}'_{lab} \\
\mathbf{q}^2_{lab} &= (\vec{q})^2 = (\vec{k_{lab}} - \vec{k'_{lab}})^2 = \mathbf{k}^2_{lab} + \mathbf{k}'^2_{lab} - 2\mathbf{k}_{lab}\mathbf{k}'_{lab} cos\theta_{e_{lab}} \\
Q^2 &= -q^2 = 4\mathbf{k}_{lab}\mathbf{k}'_{lab} sin^2\frac{\theta_{e_{lab}}}{2} \\
s &= (p+q)^2 = m^2 - Q^2 + 2mq^0_{lab} \\
\epsilon &= \frac{1}{1 + 2\frac{\mathbf{q}^2_{lab}}{Q^2} tan^2\frac{\theta_{e_{lab}}}{2}} \\
\mathbf{q}^2 &= Q^2 + \frac{(s - Q^2 - m^2)^2}{4s} \\
\mathbf{q}' &= \frac{s - m^2}{2\sqrt{s}}
\end{aligned} \tag{11}$$

The first goal of the experiment method is to study $\mathcal{M}^{exp}$ at fixed $(\mathbf{q}, \epsilon, \theta, \varphi)$ as a function of $\mathbf{q}'$. The kinematics of table 3 show that in order to maintain ϵ constant when $\mathbf{q}$ is fixed, and $\mathbf{q}'$ varies from 21.5 MeV to 111.5 MeV, we have to change the incident electron energy $(\mathbf{k}_{lab})$.

$\mathbf{q}$ **MeV**	$\mathbf{q}'$ **MeV**	ϵ		$\mathbf{k}_{lab}$ **GeV**	$\mathbf{k}'_{lab}$ **GeV**	$\theta_{e_{lab}}$ **deg**	$\theta_{\gamma^{virtual}_{lab}}$ **deg**
600	111.5	0.62		.855	.5394	52.2	-39.1
600	21.5	0.72		.855	.654	45.7	-49.6
600	21.5	0.62		.735	.534	55.2	-45.5

Table 3: *Variation of* $\mathbf{k}_{lab}$ *with* ϵ*, when* $\mathbf{q}$ *is fixed, and* $\mathbf{q}'$ *varies from 21.5 MeV to 111.5 MeV*

Therefore the incident electron energy and the nominal angle and momentum of the electron spectrometer are chosen for the 5 $\mathbf{q}'_{ref}$ measurements as it is indicated in table 4.

Since the electron spectrometer has a finite acceptance in angle and momentum, we access in a measurement to a finite domain of $(\mathbf{q}, \mathbf{q}', \epsilon)$ values (see figure 8, 9). We can define an acceptance in $\mathbf{q}'$ for the good events such as :

$$\mathbf{q}' = \mathbf{q}'_{ref} \pm 15\ MeV$$

Then the acceptances in $\mathbf{q}$ and ϵ for all the $\mathbf{q}'_{ref}$ measurements are the same and are such as :

$$\mathbf{q} = (600 \pm 20)\ MeV\ ;\ \epsilon = 0.62 \pm 0.02$$

In the analyzis (calculations of $\mathcal{M}_{-2}, \mathcal{M}_{-1}, \mathcal{M}_0$) we will have to take into account all these acceptances.

q **MeV**	**q**$'$ **MeV**	ϵ		**k**$_{lab}$ **GeV**	**k**$'_{lab}$ **GeV**	$\theta_{e_{lab}}$ **deg**	$\theta_{\gamma^{virtual}_{lab}}$ **deg**
600	111.5	0.62		.855	.539	52.2	-39.1
600	90.0	0.62		.825	.538	53.0	-40.6
600	67.5	0.62		.795	.537	53.8	-42.2
600	45.0	0.62		.765	.535	54.5	-43.8
600	21.5	0.62		.735	.534	55.2	-45.5

Table 4: *Kinematics chosen in this experiment in order to maintain* ***q****,* ϵ *constant, when 5 values of* ***q'*** *are selected between 21.5 MeV and 111.5 MeV*

In order to separate $P_{LL}(\mathbf{q})$ and $P_{TT}(\mathbf{q})$, we need at least 2 different values of ϵ. At fixed value of $\mathbf{q}$, the smallest value of ϵ is determined by the maximum angle of the electron spectrometer ($\theta_{e_{lab}} \leq 63.14°$) (see table 5). However the lever arm for a good separation with these two extreme polarisations $\epsilon_1 = 0.62$, $\epsilon_2 = 0.54$ will be really small, and in a first experiment we will consider only one polarization ($\underline{\epsilon_1 = 0.62}$).

q **MeV**	**q**$'$ **MeV**	ϵ		**k**$_{lab}$ **GeV**	**k**$'_{lab}$ **GeV**	$\theta_{e_{lab}}$ **deg**	$\theta_{\gamma^{virtual}_{lab}}$ **deg**
600	111.5	0.62		.855	.539	52.2	-39.1
600	21.5	0.62		.735	.534	55.2	-45.5
600	111.5	0.54		.750	.464	59.5	-36.3
600	21.5	0.54		.660	.459	63.6	-42.0

Table 5: *Variation of* $\theta_{e_{lab}}$ *with* ϵ*, when* ***q*** *is fixed, and* ***q'*** *varies from 21.5 MeV to 111.5 MeV*

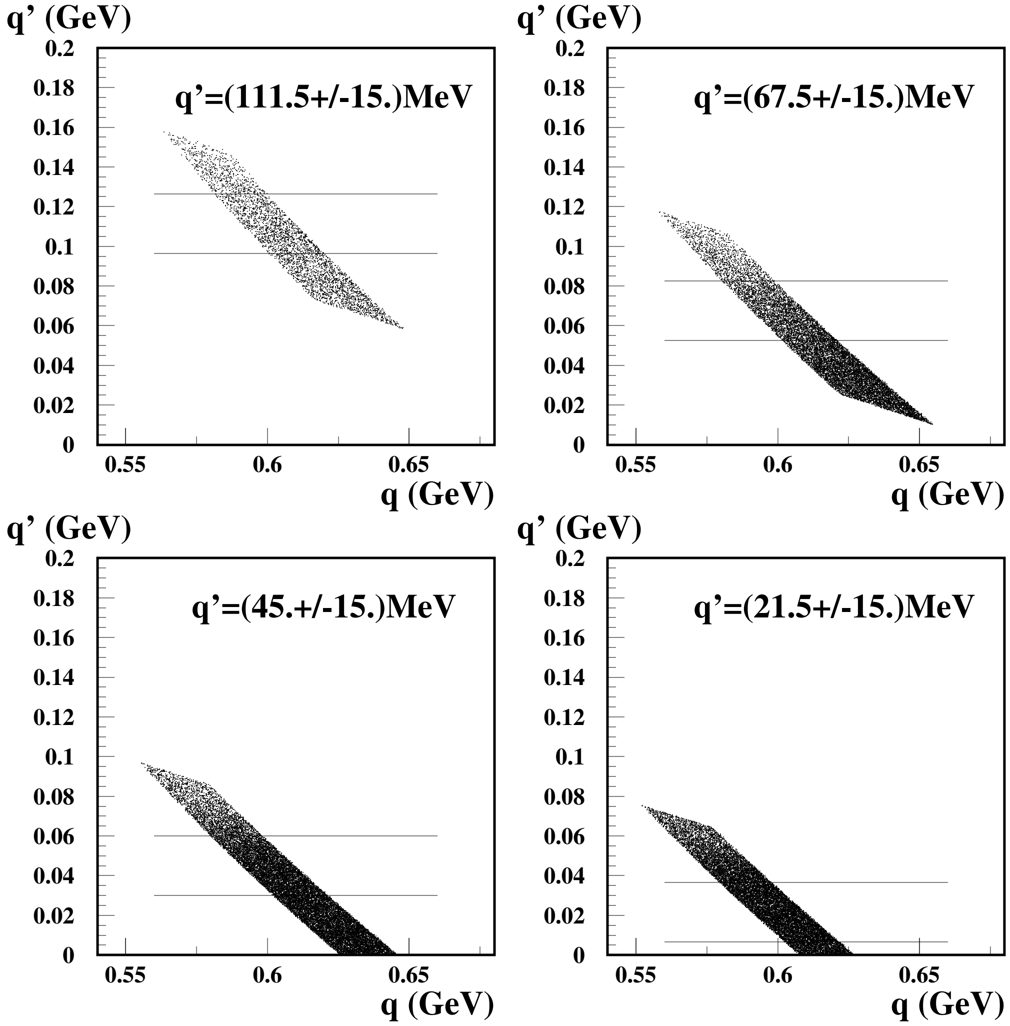

Figure 8: *Exemples of domains in* $\boldsymbol{q}$ *and* $\boldsymbol{q'}$ *accessed in 4* $\boldsymbol{q'}_{ref}$ *measurements according to the acceptance of the electron spectrometer. For each setup, we will select only the good events in the range :* $\boldsymbol{q'}_{ref} - 15.\ MeV \leq \boldsymbol{q'} \leq \boldsymbol{q'}_{ref} + 15.\ MeV$*, then* $\boldsymbol{q} = (600 \pm 20)\ MeV$.

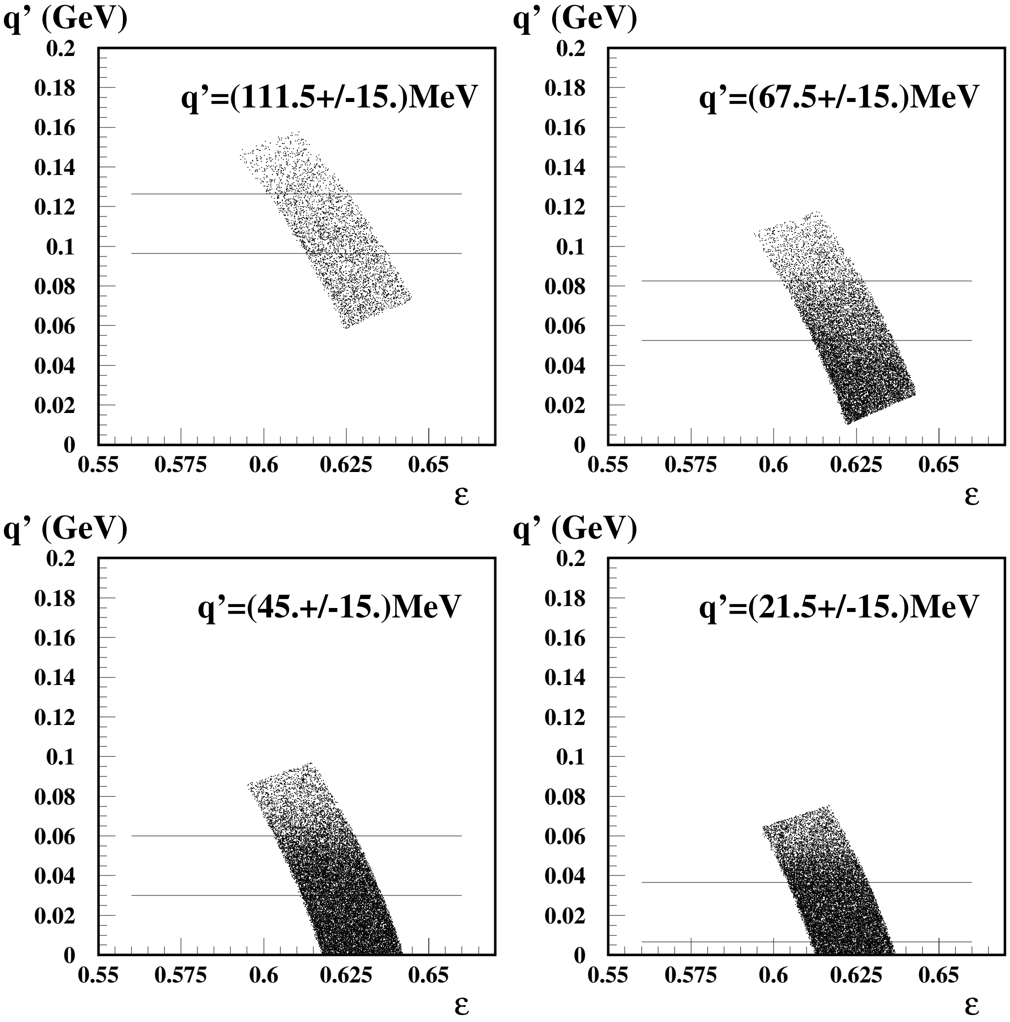

Figure 9: *Exemples of domains in* ϵ *and* q' *accessed in 4* q'_{ref} *measurements according the acceptance of the electron spectrometer. For each setup, we will select only the good events in the range :* $q'_{ref} - 15.\ MeV \leq q' \leq q'_{ref} + 15.\ MeV$*then* $\epsilon = (0.62 \pm 0.02)$.

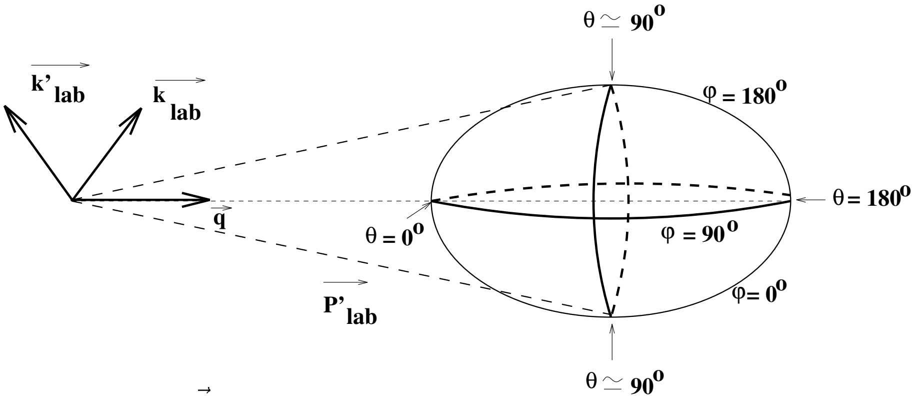

Figure 10: *Evolution of* $\vec{p'}_{lab}$ *due to Lorentz Boost. The extremity of the momentum vector* $\vec{p'}_{lab}$ *describes the surface of a rugby ball.* $\mathbf{p'}_{lab}$ *is smallest (largest), when the outgoing photon is in the forward (backward) direction :* $\theta = 0°$ *(180°). The angle between* $\vec{p'}_{lab}$ *and* $\vec{q}_{lab}$ *is largest when the angle of the outgoing photon in the CM is around* $\theta = 90°$*. The reference* $\varphi = 0°$ *is defined when the real photon is in the electronic plane, in the same half-plane than the incident and scattered electrons.*

3.1.2 Definition of the hadronic arm according to θ, φ

The second step of the experimental method is to investigate the $e + p \rightarrow e' + p' + \gamma$ reaction in a large domain of (θ, φ). Due to the CM to *lab* Lorentz boost, the outgoing proton momentum is focused in a small cone around the virtual photon momentum while the outgoing real photon describes all the space (see figure 10). The parallels on the rugby ball correspond to different values of θ, and the meridians to different values of φ. The $\mathbf{p'}_{lab}$ and $\theta^{\gamma p}_{lab}$ variations are indicated as a function of $\theta^{\gamma\gamma}_{lab}$ on the polar plots in figures 11 and 12. It is clear that the variation in momentum and angle of the outgoing proton when the real photon describes all the space is larger when $\mathbf{q'}$ is larger. The combination of the two pieces of information momentum and angle of the outgoing proton is represented in figure 13 for $\mathbf{q'} = 111.5$ MeV. Each point $(\mathbf{p'}_{lab}, \theta_{p_{lab}})$ on this plot corresponds to precise values in (θ,φ) as it is clearly indicated. In order to collect all the values in (θ, φ), we have to position the proton spectrometer at one or several nominal values in $(\mathbf{p'}_{lab}, \theta_{p_{lab}})$ in order to cover all the domain because of the finite acceptances in momentum and angle of the spectrometer. In figure 13, we have also represented two particular kinematical points $(\theta_{p_{lab}}, \mathbf{p'}_{lab})$ corresponding to the cases $(\vec{q'}//\vec{k})$ and $(\vec{q'}//\vec{k'})$ where the BH process is dominant and reduced completly any effect of the "generalized polarizabilities" : so the choice of these region will be preferentially avoided. The choice of the different setup is presented in figures 14 and 15 and in table 6 for the different values of $\mathbf{q'}$.

If we consider that the proton spectrometer moves only in the leptonic plane, we can not access protons which are emited too far above or below the leptonic plane because of its finite vertical acceptance (70 mrad) (central area in figure 13). It is the reason why we have chosen preferentially the setup along $\varphi = 0°$ or $180°$ in the promising region far from the incident and scattered electron directions.

At small $\mathbf{q'}$ (45. MeV and 21.5 MeV), the rugby ball is smaller and can be easily intercepted in the spectrometer acceptance. Nevertheless it is necessary to avoid the large contribution of the elastic peak.

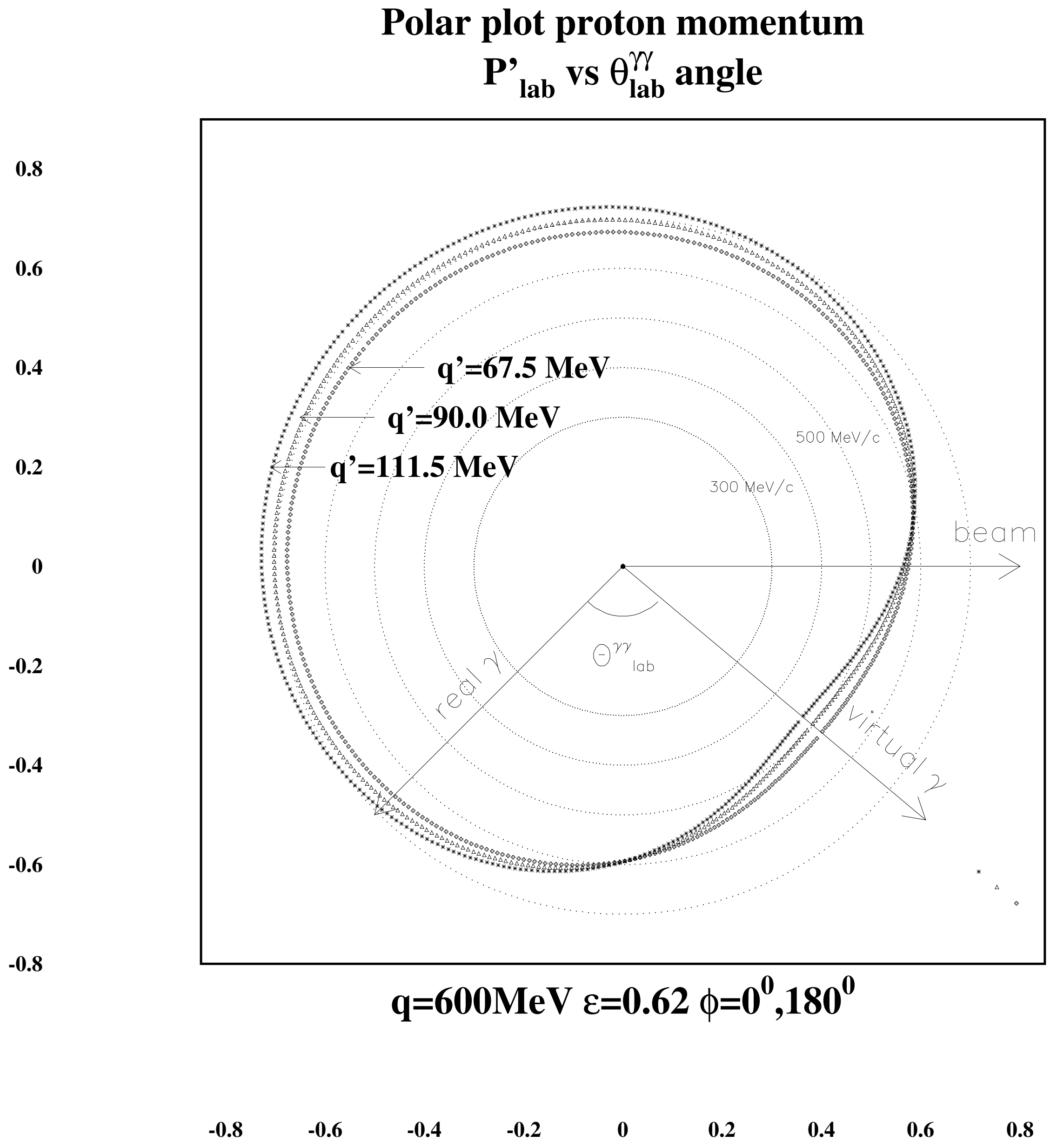

Figure 11: *Polar plot* $\boldsymbol{p'}_{lab}$ *vs* $\theta^{\gamma\gamma}_{lab}$ *at* $\boldsymbol{q} = 600$ *MeV*, $\epsilon = 0.62$, $\varphi = 0°$ *or* $180°$ *and* $\boldsymbol{q'}$ = *67.5, 90, 111.5 MeV. For given (*$\boldsymbol{q}$, $\boldsymbol{q'}$, ϵ*), the incident electron, scattered electron and virtual photon directions are completly defined ; on this figure at* $\varphi = 0°$ *or* $180°$*, we have indicated the incident electron and virtual photon axes. As* $\theta^{\gamma\gamma}_{lab}$ *varies from* $-180°$ *to* $180°$*, the real photon direction turns around the virtual photon direction. The proton momentum modulus is reported on each radius corresponding to the direction of the real photon.*

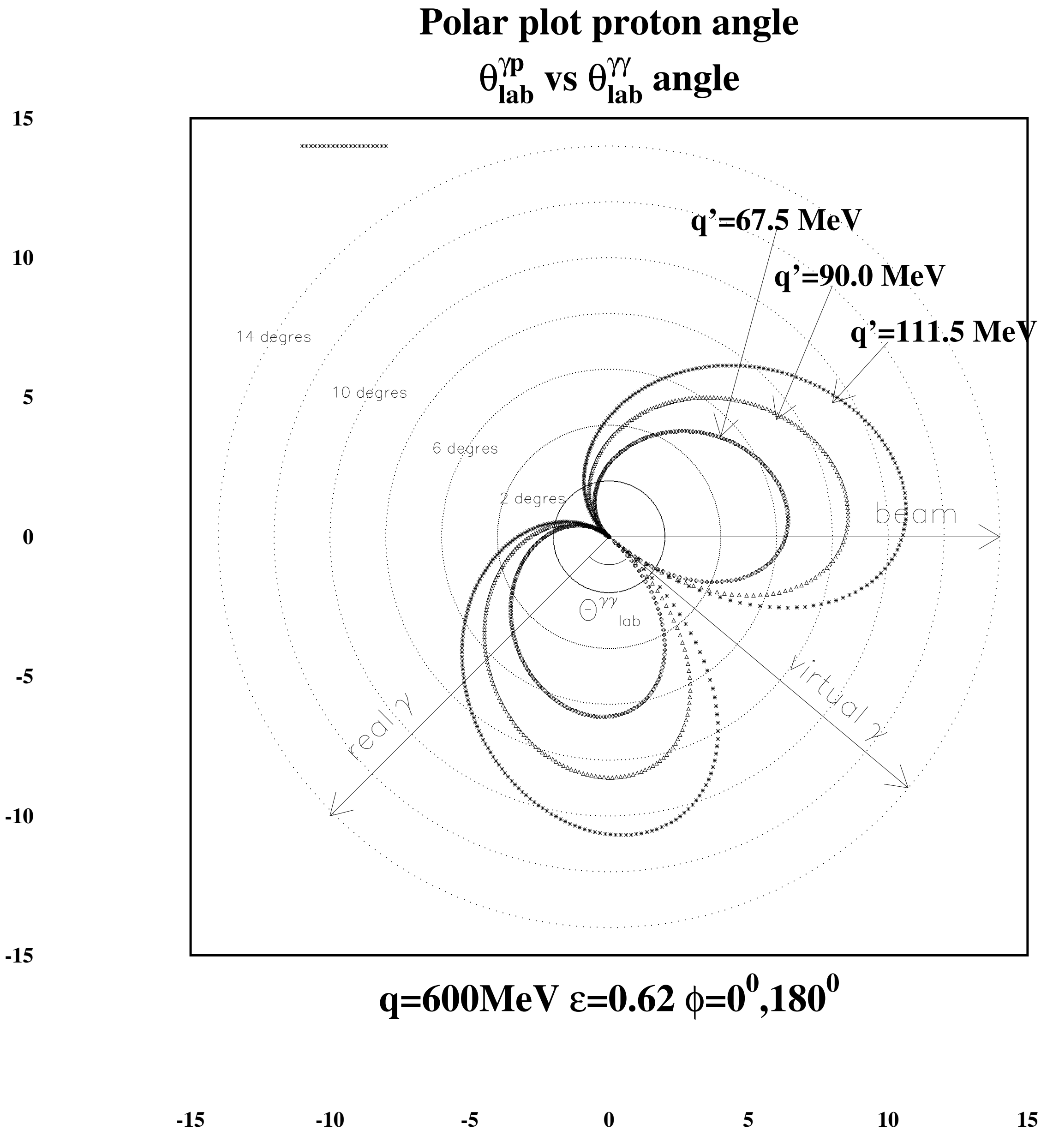

Figure 12: *Polar plot* $\theta^{\gamma p}_{lab}$ *vs* $\theta^{\gamma\gamma}_{lab}$ *at* $\boldsymbol{q} = 600$ *MeV*, $\epsilon = 0.62$, $\varphi = 0°$ *or* $180°$ *and* $\boldsymbol{q'} =$ *67.5, 90, 111.5 MeV. For given* ($\boldsymbol{q}$, $\boldsymbol{q'}$, ϵ)*, the incident electron, scattered electron and virtual photon directions are completly defined ; on this figure at* $\varphi = 0°$ *or* $180°$*, we have indicated the incident electron and virtual photon axes. As* $\theta^{\gamma\gamma}_{lab}$ *varies from* $-180°$ *to* $180°$*, the real photon direction turns around the virtual photon direction. The proton angle with the virtual photon direction is reported on each radius corresponding to the direction of the real photon.*

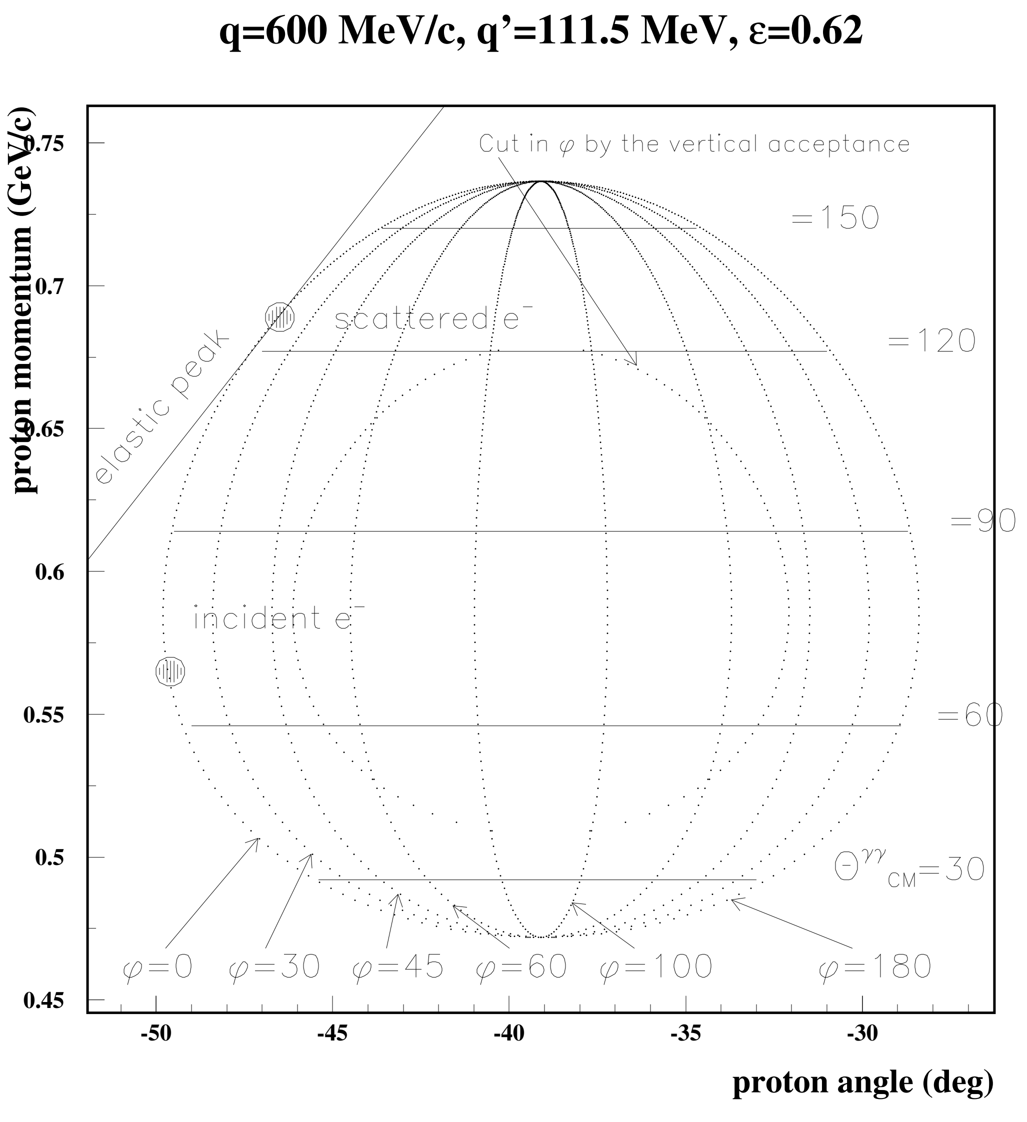

Figure 13: *The combination of the two pieces of information, momentum and angle, of the outgoing proton for* $\boldsymbol{q'}$ = 111.5 *MeV. Each point* ($\boldsymbol{p'}_{lab}, \theta_{p_{lab}}$) *corresponds to precise values in* (θ, φ)*. The central area represents the domain which will not be accessible with a proton spectrometer moving only in the plane* $\varphi = 0°$ *and with a finite vertical acceptance* ($\pm 70 mrad$)*.*

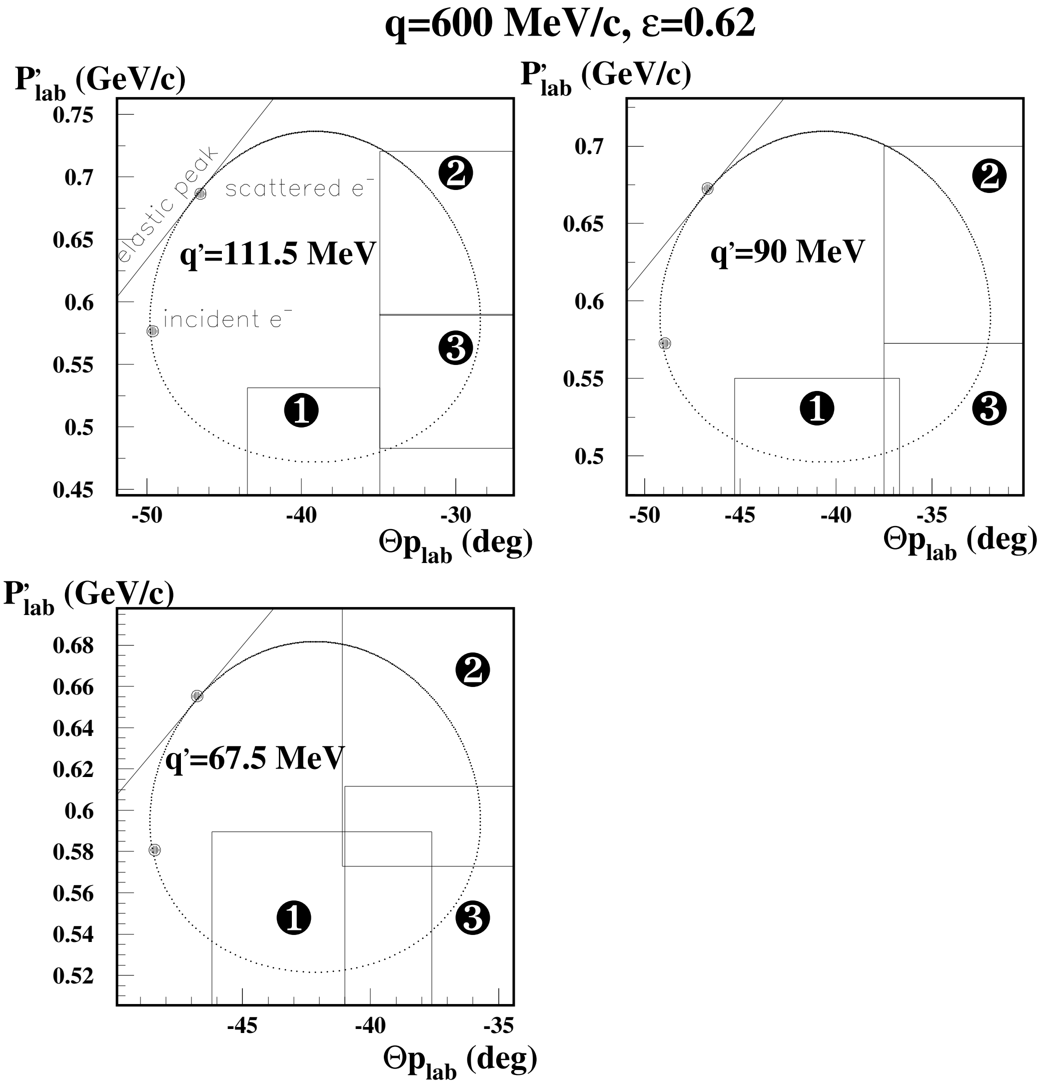

Figure 14: *Choice of the different setup (represented by each box) in order to cover at best all the domain in* $(\mathbf{p}'_{lab}, \theta_{p_{lab}})$ *for the larger values of* $\mathbf{q}'$. *Because of finite vertical acceptance of the spectrometer, we have chosen preferentially the setup along* $\varphi = 0°$ *or* $180°$ *in the promising region far from the incident and scattered electron directions.*

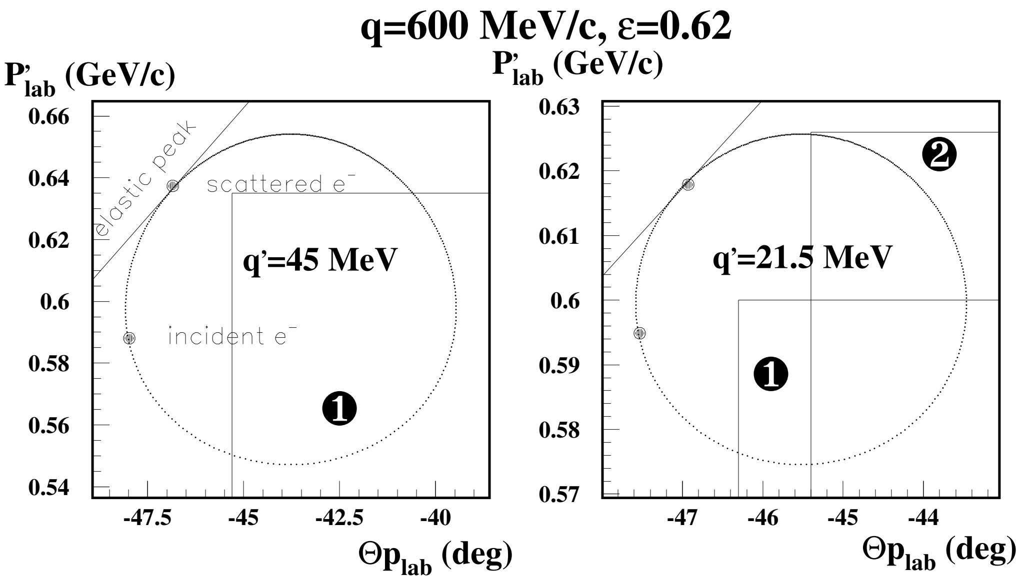

Figure 15: *Choice of the different setup (represented by each box) in order to cover at best all the domain in* ($\boldsymbol{p}'_{lab}, \theta_{p_{lab}}$) *for the smaller values of* $\boldsymbol{q}'$. *The rugby ball is smaller and can be easily intercepted in the spectrometer acceptance. Nevertheless it is necessary to avoid the large contribution of the elastic peak.*

$\mathbf{q}$ MeV	$\mathbf{q}'$ MeV	ϵ	N^0	$\mathbf{k}_{lab}$ GeV	$\mathbf{k}'_{lab}$ GeV	$\theta_{e_{lab}}$ deg	$\mathbf{p}'_{lab}$ GeV	$\theta_{p_{lab}}$ deg
600	111.5	.62	1	.855	.5394	52.18	.4830	-39.2
600	111.5	.62	2	.855	.5394	52.18	.6550	-30.6
600	111.5	.62	3	.855	.5394	52.18	.5364	-30.6
600	90.0	.62	1	.825	.5375	53.02	.5000	-41.0
600	90.0	.62	2	.825	.5375	53.02	.6364	-33.2
600	90.0	.62	3	.825	.5375	53.02	.5210	-33.2
600	67.5	.62	1	.795	.5365	53.78	.5360	-41.9
600	67.5	.62	2	.795	.5365	53.78	.6364	-36.8
600	67.5	.62	3	.795	.5365	53.78	.5560	-36.8
600	45.0	.62	1	.765	.5348	54.52	.5770	-41.0
600	21.5	.62	1	.735	.5337	55.17	.5450	-42.0
600	21.5	.62	2	.735	.5337	55.17	.5630	-41.1

Table 6: *Kinematics chosen in this experiment for the proton spectrometer, when 5 values of* q' *are selected between 21.5 MeV and 111.5 MeV*

3.2 Counting rate estimation

We have used a simulation of the experiment, which has been well controlled with the help of a first experimental test (realized in March 1995).

The Monte Carlo simulation takes into account :

- momentum resolution on $\mathbf{k}_{lab}$, $\mathbf{k}'_{lab}$, $\mathbf{p}'_{lab}$,
- angular resolution on $\theta_{e_{lab}}$, $\theta_{p_{lab}}$,
- Coulomb multiple scattering in target and target wall for incident and scattered electrons and recoil proton,
- radiative corrections have been roughly taken into account by allowing incident and scattered electrons to radiate a second photon. The angular peaking approximation and the equivalent radiator for internal bremsstrahlung have been used. This equivalent radiator is on the order of 2% to 3% of radiation lenght in our energy domain. As the target represents only 2×10^{-3} radiation lenght (and 0.4×10^{-3} radiation lenght for the target wall), we neglect the external radiative corrections compared to the internal one.

In order to evaluate the good event counting rate, we have introduced in the simulation the cross section given by $|T^{Born} + T^{BH}|^2$ for the Virtual Compton Scattering and the Bethe-Heitler processes, which are the first orders of the total contribution. The single rates for electron and proton coming from target and target wall have been measured in the first experimental test which investigated a few kinematical conditions.

The table 7 summarizes for each kinematical condition the single electron and proton rates and the good coincidence rate. These rates are given in counts per second for a luminosity of 10^{37} cm^{-2} s^{-1}, which corresponds to a 20 μA beam current on a 2 cm length liquid hydrogen target.

"N_{good}" indicates the number of "good events" in the range

$$\mathbf{q}'_{ref} - 15.MeV \leq \mathbf{q}' \leq \mathbf{q}'_{ref} + 15.MeV$$

and with a angular rejection for the real photons which are emitted in a cone of 30° opening angle around the direction of the incident or scattered electrons. The promising region to maximize the effect of the polarisabilities is obviously outside these two directions.

3.3 Feasibility of the experiment

3.3.1 Accidental background in the coincidence time

The large duty cycle and the requirement of a correlation in time, space and missing mass ensure a very acceptable level of accidental coincidence. This is clearly shown in the experimental coincidence time spectrum of figure 16 which has been obtained in the kinematical conditions of the setup $N°$ 1 for $\mathbf{q}' = 111.5MeV$. This spectrum has been corrected for all the various trajectory lengths and the offset of the different time-of-flight scintillators in the spectrometer focal plane. The resulting coincidence time resolution is 1.15 ns, and the ratio between the number of good events in the peak and the number of accidental coincidences in 3 ns is 22! This experimental value is reproduced by our estimations, and for all the setup, the ratio remains larger than 10.

3.3.2 Experimental resolution in missing mass

Figure 17 shows the very good separation in missing mass of the reaction $p(e,e'p)X$. The Compton events ($m_X^2 = 0$ MeV^2) and the π^0 electroproduction events ($m_X^2 = m_{\pi^0}^2 = 18214$ MeV^2) are well separated. The width ($FWHM$) of the Compton peak is determined by the very good resolution of the device (beam and spectrometers), the multiple scattering in the target and slightly by the radiative corrections. The estimated resolving power $m_{\pi^0}^2/FWHM$ is always larger than 15 for all the setup.

3.4 Limitations of the experiment

3.4.1 Acquisition system

100 evts/s seems a reasonable limitation of the present acquisition system, but the coincidence rate in the foreseen kinematics (presented in table 7) is always smaller than 5s^{-1}.

$\mathbf{q} = .600\,GeV$ $\mathbf{q}' = .1115\,GeV,\ \epsilon = .62,\ \mathbf{k}_{lab} = .855\,GeV$								
N^0	electron		proton		Single rate (s^{-1})		Good coincidence rate (s^{-1})	
	$\theta_{e_{lab}}$	$\mathbf{k}'_{lab}$	$\theta_{p_{lab}}$	$\mathbf{p}'_{lab}$	N_e	N_p	N_{t}	N_{good}
1	52.18	.5394	-39.2	.4830	1600	83000	0.126	0.067
2	52.18	.5394	-30.6	.6550	1600	60000	0.159	0.086
3	52.18	.5394	-30.6	.5364	1600	104000	0.061	0.043
$\mathbf{q} = .600\,GeV$ $\mathbf{q}' = .090\,GeV,\ \epsilon = .62,\ \mathbf{k}_{lab} = .825\,GeV$								
1	53.02	.5375	-41.0	.5000	1900	65000	0.265	0.112
3	53.02	.5375	-33.2	.6364	1900	50000	0.264	0.153
2	53.02	.5375	-33.2	.5210	1900	80000	0.083	0.057
$\mathbf{q} = .600\,GeV$ $\mathbf{q}' = .0675\,GeV,\ \epsilon = .62,\ \mathbf{k}_{lab} = .795\,GeV$								
1	53.78	.5365	-41.9	.5360	2100	49000	0.750	0.305
2	53.78	.5365	-36.8	.6364	2100	39000	0.685	0.375
3	53.78	.5365	-36.8	.5560	2100	59000	0.230	0.195
$\mathbf{q} = .600\,GeV$ $\mathbf{q}' = .045\,GeV,\ \epsilon = .62,\ \mathbf{k}_{lab} = .765\,GeV$								
1	54.52	.5348	-41.0	.5770	2700	45000	2.470	1.165
$\mathbf{q} = .600\,GeV$ $\mathbf{q}' = .0215\,GeV,\ \epsilon = .62,\ \mathbf{k}_{lab} = .735\,GeV$								
1	55.17	.5337	-42.0	.5450	3900	41000	2.470	1.290
2	55.17	.5337	-41.1	.5630	3900	41000	2.940	1.740

Table 7: *Single rate for protons (N_p) and electrons (N_e) and coincidence rate (N_t) in counts/s^{-1} for each setup. All the counting rates are obtained for a 20 μA beam current on a 2 cm length liquid hydrogen target : £ = 10^{37} cm^{-2} s^{-1}. We have also included the rate N_{good} obtained with the kinematical condition $\mathbf{q}'_{ref} - 15\ MeV \leq \mathbf{q}' \leq \mathbf{q}'_{ref} + 15\ MeV$ and the angular rejection for the real photons which are emitted in a cone of 30° opening angle around the direction of the incident or scattered electrons.*

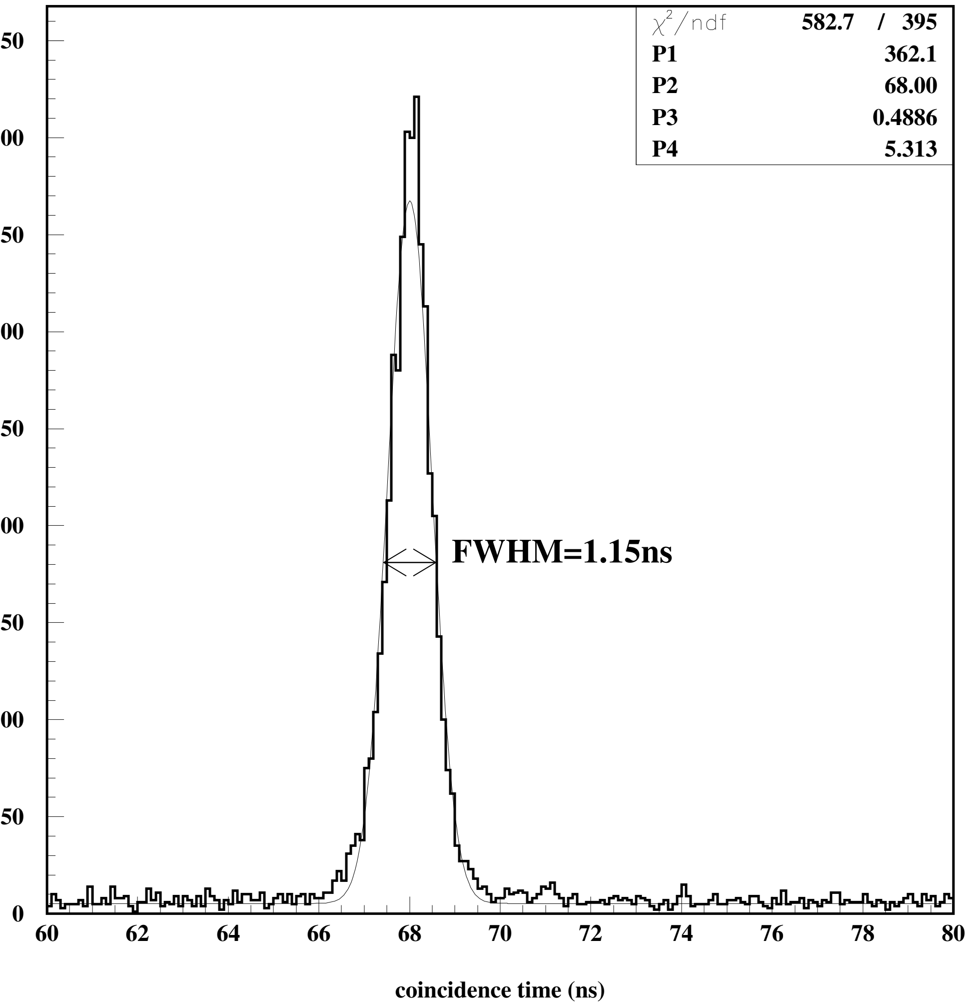

Figure 16: *Experimental coincidence time spectrum which has been obtained in the kinematical conditions of the setup* N° *1 for* $q' = 111.5 MeV$.

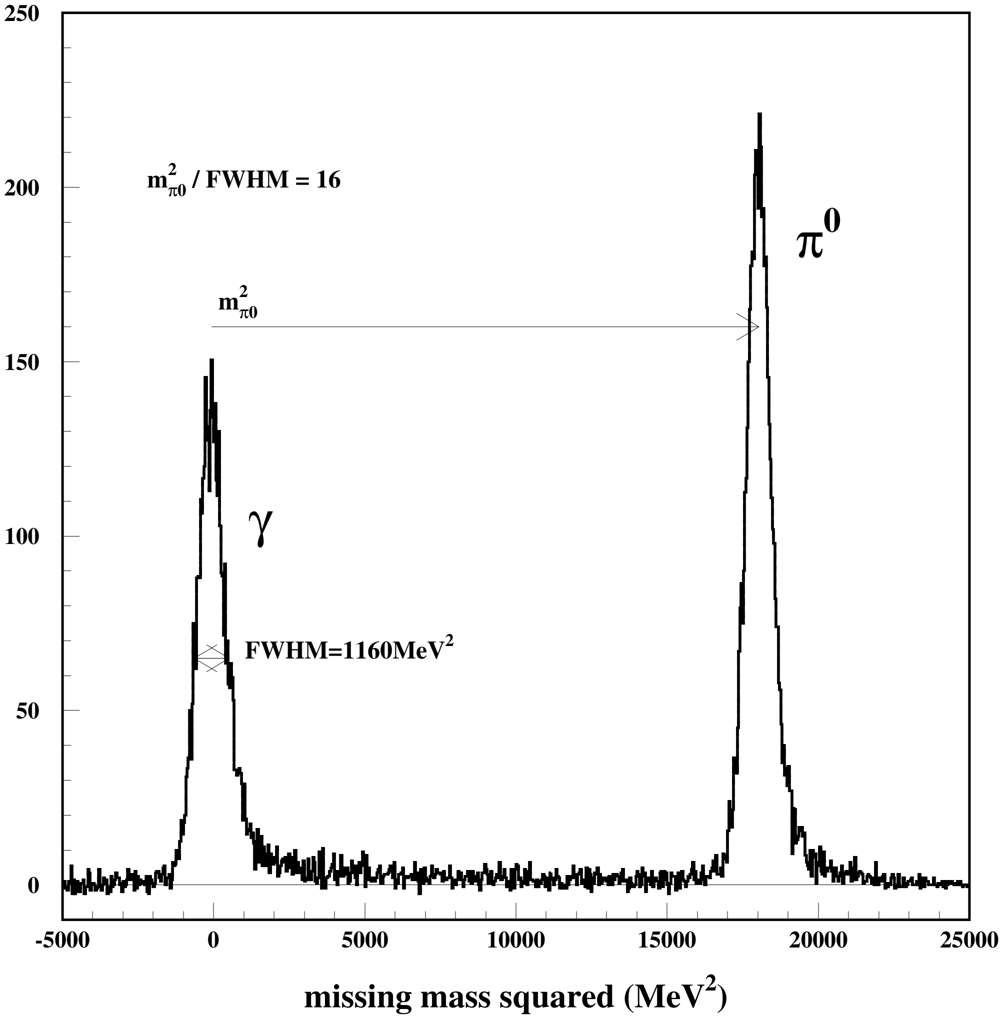

Figure 17: *The experimental spectrum of the missing mass (in* MeV^2*) in the reaction* $p(e,e'p)X$ *with a very good separation between Compton and* π^0 *electroproduction events. This spectrum has been obtained in the kinematical conditions of the setup N° 1 for* $q' = 111.5 MeV$.

3.4.2 Elastic peak contribution

The elastic peak could provide really larger contributions than 100 evts/s. The elastic events which are in coincidence in electron and proton spectrometers are parasitic events. They are correlated in time, space and give a good missing mass value. It is necessary to get rid of this elastic contribution. In order not to increase considerably the number of events, the promising proton setup for the purposed study is always chosen sufficiently far from the elastic peak position (see figures 14 and 15).

3.4.3 Beam intensity on the cryogenic target

All the counting rates have been estimated with a luminosity $\pounds = 10^{37}$ cm^{-2} s^{-1} which corresponds to a 20 μA beam current on a 2 cm length liquid hydrogen target. In the previous test, we have investigated in detail the evolution of the hydrogen target density as a function of the beam current. It is clear that at 60μA, the density loss is of the order of 1 or 2%. So we can used a beam current between 20 and 60μA.

3.4.4 Number of protons detected in the vertical drift chambers

A main limitation of the electron beam current is the number of protons reaching the vertical drift chambers in the proton spectrometer focal plane. They create an excessively high chamber current which can damage considerably the chamber life time. This limitation is a chamber curent of 6 μA. It corresponds to ~100000 events detected in the proton spectrometer focal plane (for proton momentum around 600 MeV/c). So we see in table 7, that the number of single protons allows one to increase at maximum in some kinematical setup, the beam current by a factor 2.5

3.4.5 Target wall contribution

We can measured precisely the iron target wall contribution with an empty target, or we can separate this contribution with the help of the very accurate vertex reconstruction thanks to the Clam "B" spectrometer. As it is shown in figure 18, a 1.4 cm central part of the target can be selected in order to avoid the wall target contribution. The used target length has to be very well controlled by the reaction $ep \rightarrow ep$. Nevertheless it is necessary to verify at least one time this method with a real empty target.

SUMMARY : Choice of kinematics and beam time request

We summarize the choice of the different kinematics in table 6 and their corresponding counting rates in table 7.

For each change of the electron beam, it is necessary to study the precise value of the beam intensity, the target density and the target length with the elastic reaction $ep \rightarrow ep$ in order to determine with a good accuracy the luminosity.

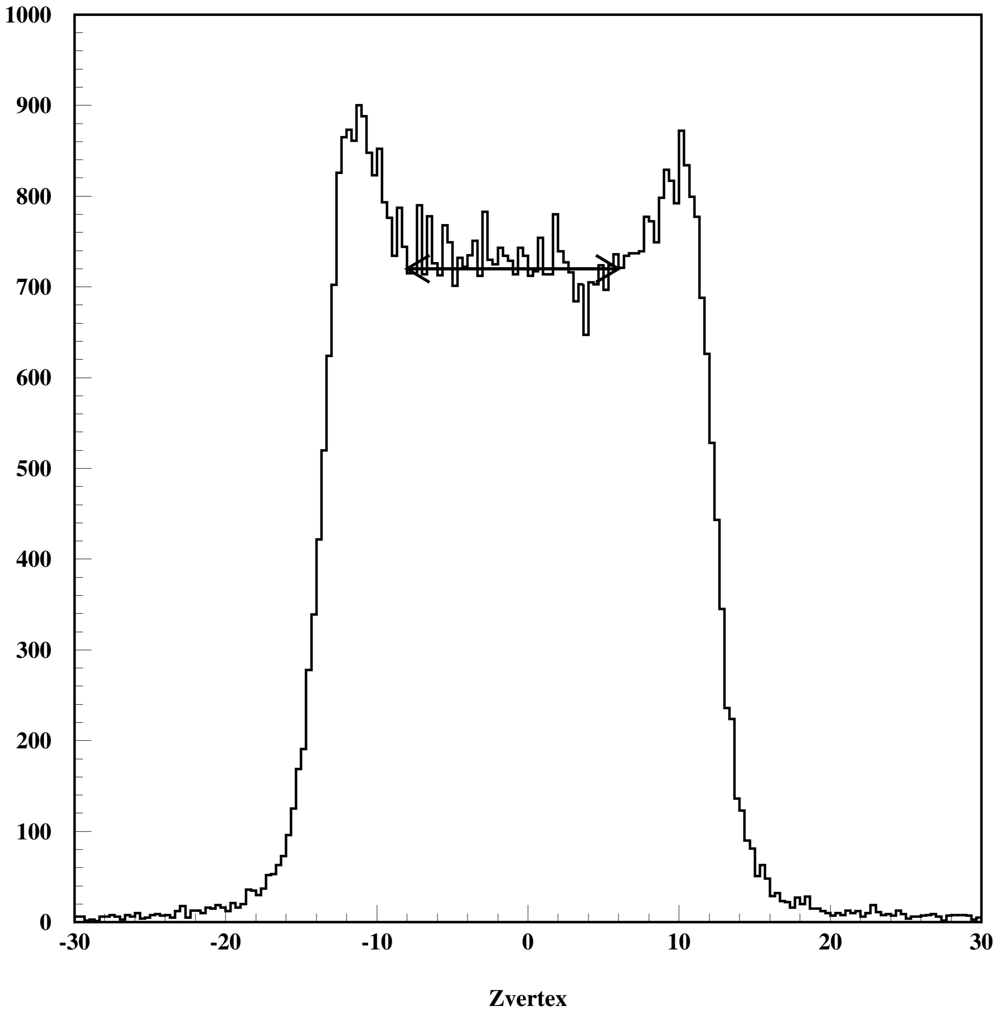

Figure 18: *The experimental reconstructed vertex of the events for good electrons and protons selected respectively in the "B" and "A" spectrometers. In order to avoid the contribution of the target wall, we can only consider the central part of the target (indicated by the arrow) where the event number is constant.*

As our goal is to investigate the $e+p \to e'+p'+\gamma$ reaction in a large domain of (θ, φ), it is necessary to have good statistics ($\sim$ 1000 events) in small bins ($\Delta\theta \sim 10°, \Delta\varphi \sim 10°$) (for which the size has to be compatible with the expected experimental resolution). The polarizabilities which give deviation of the order of 10% respectively to the BH and Born background are obtained through two succeeding fits :

- a first one, realized in all the cells (θ, φ) on the 5 values in **q'**, will provide $\mathcal{M}_{-2}^{exp}(\theta, \varphi)$, $\mathcal{M}_{-1}^{exp}(\theta, \varphi)$, $\mathcal{M}_{0}^{exp}(\theta, \varphi)$,
- a second one, is done with the formula (10) on all the values of $(\mathcal{M}_0^{exp} - \mathcal{M}_0^{LET})(\theta, \varphi)$ obtained in each cell in order to extract 3 quantities directly related to the "generalized polarizabilities".

According to the values N_{good} of "good events" counting rates, a used hydrogen lenght target of 1.4 cm, and a maximum courant (20 to 50μA depending of the setup) we need :

183 hours for $\mathbf{q}'$=111.5 MeV

140 hours for $\mathbf{q}'$=90.0 MeV

72 hours for $\mathbf{q}'$=67.5 MeV

35 hours for $\mathbf{q}'$=45.0 MeV

21 hours for $\mathbf{q}'$=21.5 MeV

In conclusion we will measure for the first time the "generalized polarizabilities" at $\mathbf{q}$=600 MeV or Q^2=0.33 GeV^2 with 450 hours of beam time.

4 Outlook

The present experiment allows, a priori, the determination of 4 combinations of polarizabilities. To determine the other combinations, one needs to use both polarized electrons and polarized target (or equivalently one needs to detect the polarization of the recoil proton). In view of the difficulty of such experiments, we postpone this study until the theoretical guide for that has been established.

By constrast, the use of polarized beam only is almost for free and this can bring usefull informations about contaminating processes which are of higher order in α_{QED}. Below the pion threshold the photon electroproduction amplitude is hermitian as far as higher order processes, such as photon rescattering, 2 photon exchange..., are neglected. As is known, (see [9] for a detailled discussion) the combination of hermiticity and time reversal implies that the electron spin asymetry is zero. So by measuring the later we have a direct measurement of the higher order processes. Of course the asymetry still vanish when φ=0 by parity. Therefore this measurement must be done out of plane.

References

[1] P.S. Baranov *et al.*, Sov. J. Nucl. Phys. **21** (1975) 355

[2] F.J. Federspiel *et al.*, Phys. Rev. Lett. **67** (1991) 1511

[3] A. Zieger *et al.*, Phys. Lett. **B278** (1992) 34

[4] E.L. Hallin *et al.*, Phys. Rev. **C48** (1993) 1497

[5] J. Schiedmayer *et al.*, Phys. Rev. Lett. **61** (1988) 1065, Nucl. Inst. Meth. **A284** (1989) 137, Phys. Rev. Lett. **66** (1991) 1015

[6] L. Koester *et al.*, Zeit. Phys. **A329** (1988) 229

[7] P.A.M. Guichon, G. Liu, A.W. Thomas, Nucl. Phys. **A591** (1995) 606

[8] F.E. Low, Phys. Rev. **96** (1954) 1428

[9] P. Kroll, M. Schürmann, P.A.M. Guichon, preprint WU B 95-09